Published for SISSA by Springer

Received: February 14, 2018
Revised: May 21, 2018
Accepted: June 3, 2018
Published: June 18, 2018

Scrutinizing $\bar{B} \to D^*(D\pi)\ell^-\bar{\nu}_\ell$ and $\bar{B} \to D^*(D\gamma)\ell^-\bar{\nu}_\ell$ in search of new physics footprints

P. Colangelo and F. De Fazio

Istituto Nazionale di Fisica Nucleare, Sezione di Bari, Via Orabona 4, I-70126 Bari, Italy

E-mail: pietro.colangelo@ba.infn.it, fulvia.defazio@ba.infn.it

Abstract: Besides being important to determine Standard Model parameters such as the CKM matrix elements $|V_{cb}|$ and $|V_{ub}|$, semileptonic B decays seem also promising to reveal new physics (NP) phenomena, in particular in connection with the possibility of uncovering lepton flavour universality (LFU) violating effects. In this view, it could be natural to connect the tensions in the inclusive versus exclusive determinations of $|V_{cb}|$ to the anomalies in the ratios $R(D^{(*)})$ of decay rates into τ vs μ, e. However, the question has been raised about the role of the parametrization of the hadronic $B \to D^{(*)}$ form factors in exclusive B decay modes. We focus on the fully differential angular distributions of $\bar{B} \to D^*\ell^-\bar{\nu}_\ell$ with $D^* \to D\pi$ or $D^* \to D\gamma$, the latter mode being important in the case of $B_s \to D_s^*$ decays. We show that the angular coefficients in the distributions can be used to scrutinize the role of the form factor parametrization and to pin down deviations from SM. As an example of a NP scenario, we include a tensor operator in the $b \to c$ semileptonic effective Hamiltonian, and discuss how the angular coefficients allow to construct observables sensitive to this structure, also defining ratios useful to test LFU.

Keywords: Heavy Quark Physics, Quark Masses and SM Parameters, Beyond Standard Model

ArXiv ePrint: 1801.10468

https://doi.org/10.1007/JHEP06(2018)082

JHEP06(2018)082

Contents

1 Introduction

Despite the lack of new physics (NP) signals in direct searches at colliders, there are hints of physics beyond the Standard Model (SM) in a few anomalies in the flavour sector, with observables in tension with the SM predictions. In particular, tree-level semileptonic B decays unexpectedly point to violation of lepton flavour universality (LFU), since the measured ratios $R(D^{(*)}) = \dfrac{\mathcal{B}(B \to D^{(*)}\tau\bar{\nu}_\tau)}{\mathcal{B}(B \to D^{(*)}\ell\bar{\nu}_\ell)}$ reveal an anomalous deviation of semitauonic B modes with respect to μ and e ones. The HFLAV averages [1] of BaBar [2, 3], Belle [4–6] and LHCb [7] Collaboration measurements,

$$R(D) = 0.403 \pm 0.040 \pm 0.024\,, \qquad R(D^*) = 0.310 \pm 0.015 \pm 0.008\,, \tag{1.1}$$

compared to the first SM predictions $R(D) = 0.296 \pm 0.016$, $R(D^*) = 0.252 \pm 0.003$ [8] and to the updated ones $R(D) = 0.300 \pm 0.008$ [9] and $R(D^*) = 0.260 \pm 0.008$ [10],[1] show a deviation at a global 3.9σ level. In the case of $R(D^*)$, the recent Belle result $R(D^*) = 0.270 \pm 0.035(\text{stat}) \pm^{0.028}_{0.025}\,(\text{syst})$ [13] reduces the average in (1.1). The LHCb measurement $R(J/\psi) = \dfrac{\mathcal{B}(B_c^+ \to J/\psi\tau^+\nu_\tau)}{\mathcal{B}(B_c^+ \to J/\psi\mu^+\nu_\mu)} = 0.71 \pm 0.17(\text{stat}) \pm 0.18(\text{syst})$ [14] is also slightly above the range of existing predictions within SM, but for this mode the theoretical error still needs to be precisely assessed [15]. In SM the couplings of charged leptons to gauge bosons

[1]Further recent SM calculations of $R(D^*)$ can be found in [11, 12].

JHEP06(2018)082

are lepton-flavour independent, and LFU is only broken by the Yukawa interaction, hence, evidences of LFU violation in b-hadron semileptonic modes signal physics beyond SM.

There are other puzzles affecting semileptonic heavy meson decays, in particular the tension between the determinations of the CKM matrix elements $|V_{cb}|$ and $|V_{ub}|$ from inclusive and exclusive B modes. Focusing on $|V_{cb}|$, precise determinations are obtained from the exclusive $B \to D^* \ell \bar{\nu}_\ell$ and $B \to D \ell \bar{\nu}_\ell$ decays and from the inclusive $B \to X_c \ell \bar{\nu}_\ell$ mode. In $B \to D^*$ the procedure to determine $|V_{cb}|$ is based on the extrapolation of the dilepton invariant mass spectrum up to the maximum value, using as an input hadronic form factors at this kinematical point computed by lattice QCD. The FLAG averages $|V_{cb}|^{D^*}_{\rm excl} = (39.27 \pm 0.56_{\rm th} \pm 0.49_{\rm exp}) \times 10^{-3}$ and $|V_{cb}|^{D}_{\rm excl} = (40.85 \pm 0.98) \times 10^{-3}$ [9] have to be compared to $|V_{cb}|_{\rm incl} = (42.46 \pm 0.88) \times 10^{-3}$ obtained in the kinetic scheme [1].

Considering the two sets of anomalies, the past viewpoint was to invoke NP in the ratios $R(D^{(*)})$, and to attribute the inclusive/exclusive tensions in $|V_{cb}|$ and $|V_{ub}|$ to some underlying assumptions, namely the uncertainty in the quark-hadron duality ansatz adopted for the inclusive measurement. Recent studies for $|V_{cb}|$ have focused, instead, on the errors involved in the analysis of the $B \to D^* \ell \bar{\nu}_\ell$ spectrum at the maximum dilepton invariant mass. The procedure usually adopted in the experimental determinations was based on the Caprini-Lellouch-Neubert (CLN) parametrization of the $B \to D^*$ form factors [16], which uses heavy quark (HQ) symmetry relations with the inclusion of radiative and $1/m_Q$ corrections. On the other hand, the deconvoluted fully differential $\bar{B}^0 \to D^{*+} \ell^- \bar{\nu}_\ell$ decay distribution measured by Belle [17] has been fitted adopting the Boyd-Grinstein-Lebed (BGL) parametrization of the form factors [18–20], resulting in a value for $|V_{cb}|$ compatible with the inclusive one [11, 21, 22]. Although the outcome refers to a single data set, the question has been raised if the form factor parametrization provides a solution of the $|V_{cb}|$ anomaly.

The idea that a common explanation could be found for the $R(D^{(*)})$ and $|V_{cb}|$ anomalies, invoking NP, has also been put forward [23]. As an example, adding a tensor operator to the SM effective $b \to c$ semileptonic Hamiltonian, weighted by a complex lepton-flavour dependent parameter ϵ_T^ℓ, it has been shown that a difference of ϵ_T^τ with respect to $\epsilon_T^{\mu,e}$ could account for the $R(D^{(*)})$ anomaly, considering $\epsilon_T^\tau \neq 0$ and $\epsilon_T^\mu = \epsilon_T^e = 0$ [24]. Relaxing the latter assumption, inclusive and exclusive B semileptonic decays with μ and e have been scrutinized showing that, for $\epsilon_T^\mu \neq 0$ and $\epsilon_T^e \neq 0$, it is also possible to pin down a region in the parameter space $(Re(\epsilon_T^\ell), Im(\epsilon_T^\ell), |V_{cb}|)$ where the inclusive $\mathcal{B}(B^- \to X_c^0 \ell^- \bar{\nu}_\ell)$ and exclusive $\mathcal{B}(B^- \to D^{(*)0} \ell^- \bar{\nu}_\ell)$ branching fractions, as well as the spectrum $d\mathcal{B}(B^- \to D^{*0} \ell^- \bar{\nu}_\ell)/dq^2$ close to maximum q^2 are recovered [23].

Here we reconsider the two issues, the role of the form factor parametrization and the possibility of non SM effects. We focus on $B \to D^* \ell \bar{\nu}_\ell$ in the case of both light μ, e and heavy τ lepton, with the D^* decaying to $D\pi$ or $D\gamma$. The latter mode is particularly relevant for $B_s \to D_s^*$ transitions. We express the fully differential decay rate in $\bar{B} \to D^*(D\pi) \ell^- \bar{\nu}_\ell$ and $\bar{B} \to D^*(D\gamma) \ell^- \bar{\nu}_\ell$ in terms of angular coefficient functions, and show how the analysis of the two modes may shed light on the form factor parametrization. We also reconsider the NP model in [23, 24] and study the modified angular coefficients, proposing a set of sensitive observables. Other investigations focusing on the angular distributions have been carried

JHEP06(2018)082

out in [25–34]. In particular, differential distributions including subsequent τ decay have been studied in [28, 30, 32, 33]. A tensor structure appears, for example, in the effective Hamiltonian of leptoquark models, in variants of which it is possible to accommodate a few B anomalies [35–37]. Attempts for a combined explanation of the anomalies in NP frameworks can be found in [38], while the role of ew corrections has been studied in [39].

A comment is in order, concerning the differences between the modes with light and τ leptons. The final state with τ necessarily contains at least one neutrino, making the full reconstruction of τ kinematics challenging. BaBar, Belle and the first LHCb studies of semileptonic B decays to τ exploited τ decay to light leptons, with a final state involving two neutrinos. For this reason, the amplitude $\tau \to \nu X$, with $X = \ell\nu$ has been coherently included in analyses as, e.g., in [30]. An interesting path has been followed in the recent LHCb study which exploits three-prong τ decay to the visible $\pi^+\pi^-\pi^+$ final state [40]. The topology of this mode allows the precise reconstruction of the τ decay vertex well separated from the B vertex due to the τ lifetime. This improves the discrimination from the background and, due to the presence of a single neutrino in the final state, would allow the determination of the complete kinematics of the decay (up to two two-fold ambiguities). However, τ decays with both three prong $\pi^+\pi^-\pi^+$ and four prong $\pi^+\pi^-\pi^+\pi^0$ pions enter in the signal, and these two modes are treated on the basis of their known reconstruction efficiencies, so that the measurement of the kinematic variables in semitauonic B decays still represents an experimental challenge.

This is the plan of the paper. After having set the stage for the calculation, in section 3 we discuss the fully angular distributions and the properties of the angular coefficient functions. Results in SM are presented in section 4, where the effects of the form factor parametrization, in particular CLN vs BGL, are investigated. In section 5 we compare the angular coefficients in SM and in the NP model with the tensor operator. A set of observables is considered in section 6, and ratios useful to test LFU are scrutinized. Our conclusions are presented in the last section.

2 Setting the stage

We consider $\bar{B}(p_B) \to D^*(p_{D^*}, \epsilon)\ell^-(k_1)\bar{\nu}_\ell(k_2)$, where $\bar{B} \to D^*$ denotes either $\bar{B}^0 \to D^{*+}$ or $B^- \to D^{*0}$, followed by the decay $D^*(p_{D^*}, \epsilon) \to D(p_D)F(p_F)$ with $F = \pi$ or γ. For the kinematics we adopt the convention for angles and momenta as in figure 1, with lepton-pair momentum $q = k_1 + k_2 = p_B - p_{D^*}$. In the derivation, we extend to NP the procedure in [41, 42] for $F = \pi$, considering also the case $F = \gamma$.

The amplitude of the process

$$\mathcal{A}_{\rm TOT}(\bar{B} \to D^*(\to DF)\ell^-\bar{\nu}_\ell) = \mathcal{A}(\bar{B} \to D^*\ell^-\bar{\nu}_\ell)\,\frac{i}{p_{D^*}^2 - m_{D^*}^2 + i m_{D^*}\Gamma(D^*)}\,\mathcal{A}(D^* \to DF) \tag{2.1}$$

involves three factors. To describe $\bar{B} \to D^*\ell^-\bar{\nu}_\ell$ we focus on the effective Hamiltonian

$$H_{\rm eff} = \frac{G_F}{\sqrt{2}} V_{cb}\left[\bar{c}\gamma_\mu(1-\gamma_5)b\,\bar{\ell}\gamma^\mu(1-\gamma_5)\nu_\ell + \epsilon_T^\ell\,\bar{c}\sigma_{\mu\nu}(1-\gamma_5)b\,\bar{\ell}\sigma^{\mu\nu}(1-\gamma_5)\nu_\ell\right] + \text{h.c.}\,, \tag{2.2}$$

JHEP06(2018)082

consisting in the Standard Model term and in a new physics term with a tensor operator weighted by a lepton-flavour dependent complex parameter ϵ_T^ℓ.[2] This allows to write

$$\mathcal{A}(\bar{B} \to D^* \ell^- \bar{\nu}_\ell) = \frac{G_F}{\sqrt{2}} V_{cb} \left[H_\mu^{\rm SM} L^{{\rm SM}\,\mu} + \epsilon_T^\ell H_{\mu\nu}^{\rm NP} L^{{\rm NP}\,\mu\nu} \right] \tag{2.3}$$

in terms of the quark current matrix elements

$$H_\mu^{\rm SM}(m) = \langle D^*(p_{D^*}, \epsilon(m)) | \bar{c}\gamma_\mu(1-\gamma_5) b | \bar{B}(p_B) \rangle = \epsilon^{*\alpha}(m) T_{\mu\alpha}^{\rm SM} \tag{2.4}$$
$$H_{\mu\nu}^{\rm NP}(m) = \langle D^*(p_{D^*}, \epsilon(m)) | \bar{c}\sigma_{\mu\nu}(1-\gamma_5) b | \bar{B}(p_B) \rangle = \epsilon^{*\alpha}(m) T_{\mu\nu\alpha}^{\rm NP} \tag{2.5}$$

and of the lepton currents

$$L^{{\rm SM}\,\mu} = \bar{\ell}\gamma^\mu(1-\gamma_5)\nu_\ell \tag{2.6}$$
$$L^{{\rm NP}\,\mu\nu} = \bar{\ell}\sigma^{\mu\nu}(1-\gamma_5)\nu_\ell . \tag{2.7}$$

In (2.4) and (2.5) the index m of the D^* polarization vector ϵ runs over $m = \pm, 0$. In the lepton-pair rest-frame (LRF), with the D^* three-momentum along the positive z-axis, one has:

$$\begin{aligned} &p_B = (E_B, 0, 0, |\vec{p}_{D^*}|)\,, && p_{D^*} = (E_{D^*}, 0, 0, |\vec{p}_{D^*}|)\,, && q = (\sqrt{q^2}, 0, 0, 0)\,, \\ &\epsilon_\pm = \frac{1}{\sqrt{2}}(0, 1, \mp i, 0)\,, && \epsilon_0 = \frac{1}{m_{D^*}}(|\vec{p}_{D^*}|, 0, 0, E_{D^*})\,, && \end{aligned} \tag{2.8}$$

with $|\vec{p}_{D^*}| = \dfrac{\lambda^{1/2}(m_B^2, m_{D^*}^2, q^2)}{2\sqrt{q^2}}$ and $E_{D^*} = \dfrac{m_B^2 - m_{D^*}^2 - q^2}{2\sqrt{q^2}}$, λ being the triangular function. The orientation of the lepton momenta is fixed by the angles θ and ϕ as in figure 1, so that

$$\begin{aligned} k_1 &= (k_1^0, |\vec{k}_1| \sin\theta\cos\phi, |\vec{k}_1| \sin\theta\sin\phi, |\vec{k}_1|\cos\theta) \\ k_2 &= (k_2^0, -|\vec{k}_1| \sin\theta\cos\phi, -|\vec{k}_1| \sin\theta\sin\phi, -|\vec{k}_1|\cos\theta)\,. \end{aligned} \tag{2.9}$$

In terms of the D^* polarization indices one can write

$$|\mathcal{A}(\bar{B} \to D^* \ell^- \bar{\nu}_\ell)(m,n)|^2 = \frac{G_F^2}{2} |V_{cb}|^2 \left[\mathcal{H}^{\rm SM}(m,n) + \mathcal{H}^{\rm NP}(m,n) + \mathcal{H}^{\rm INT}(m,n) \right]\,, \tag{2.10}$$

where

$$\mathcal{H}^{\rm SM}(m,n) = H_\mu^{\rm SM}(m) (H^{\rm SM})^\dagger_{\mu'}(n) \mathcal{L}^{{\rm SM}\,\mu\mu'}\,, \tag{2.11}$$
$$\mathcal{H}^{\rm NP}(m,n) = |\epsilon_T|^2 \left[H_{\mu\nu}^{\rm NP}(m) (H^{\rm NP})^\dagger_{\mu'\nu'}(n) \mathcal{L}^{{\rm NP}\,\mu\nu\mu'\nu'} \right]\,, \tag{2.12}$$
$$\mathcal{H}^{\rm INT}(m,n) = \epsilon_T H_\mu^{\rm SM}(m) (H^{\rm NP})^\dagger_{\mu'\nu'}(n) \mathcal{L}_1^{{\rm INT}\,\mu\mu'\nu'} + \epsilon_T^* H_{\mu\nu}^{\rm NP}(m) (H^{\rm SM})^\dagger_{\mu'}(n) \mathcal{L}_2^{{\rm INT}\,\mu\nu\mu'}\,, \tag{2.13}$$

[2]We only consider the tensor operator, although other operators could be produced by ew renormalization-group evolution [43].

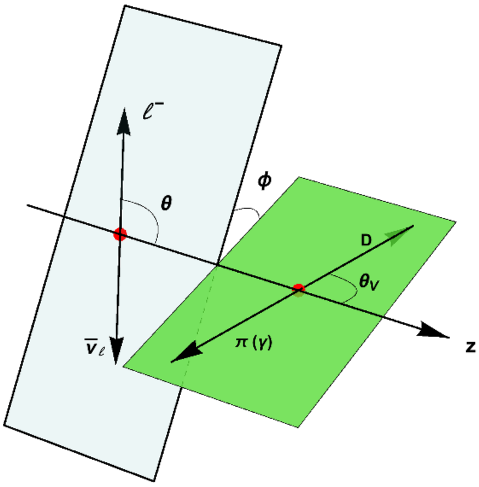

Figure 1. Kinematics of $\bar{B} \to D^*(\to DF)\ell^-\bar{\nu}_\ell$.

in terms of the quantities in (2.4), (2.5) and

$$\begin{aligned}
\mathcal{L}^{\mathrm{SM}\,\mu\mu'} &= L^{\mathrm{SM}\,\mu}(L^{\mathrm{SM}\,\mu'})^\dagger\,, \\
\mathcal{L}^{\mathrm{NP}\,\mu\nu\mu'\nu'} &= L^{\mathrm{NP}\,\mu\nu}(L^{\mathrm{NP}\,\mu'\nu'})^\dagger \\
\mathcal{L}_1^{\mathrm{INT}\,\mu\mu'\nu'} &= L^{\mathrm{SM}\,\mu}(L^{\mathrm{NP}\,\mu'\nu'})^\dagger \\
\mathcal{L}_2^{\mathrm{INT}\,\mu\nu\mu'} &= L^{\mathrm{NP}\,\mu\nu}(L^{\mathrm{SM}\,\mu'})^\dagger\,.
\end{aligned} \tag{2.14}$$

As for the D^* propagator, the narrow-width approximation can be used for the state produced nearly on-shell [44],

$$\frac{1}{(p_{D^*}^2 - m_{D^*}^2) + m_{D^*}^2\Gamma(D^*)^2} = \frac{\pi}{m_{D^*}\Gamma(D^*)}\,\delta(p_{D^*}^2 - m_{D^*}^2)\,. \tag{2.15}$$

On the other hand, the $D^* \to DF$ amplitude can be written as

$$\mathcal{A}(D^* \to DF) = g_{D^*DF}\ (\epsilon \cdot Q) \tag{2.16}$$

where $Q = p_D$ for $F = \pi$, and $Q_\beta = i\,\epsilon_{\alpha\beta\sigma\tau}\eta^{*\alpha}p_{D^*}^\sigma p_D^\tau$ for $F = \gamma$, with η the photon polarization vector. One can get rid of the coupling g_{D^*DF} considering

$$\Gamma(D^* \to DF) = g_{D^*DF}^2\frac{|\vec{p}_D|}{24\pi m_{D^*}^4}\left[(p_{D^*}\cdot Q)^2 - Q^2 m_{D^*}^2\right]\,, \tag{2.17}$$

with $|\vec{p}_D| = \dfrac{\lambda^{1/2}(m_{D^*}^2, m_D^2, m_F^2)}{2m_{D^*}}$ the D three-momentum in the D^* rest frame (D^*RF). In particular, one has $\left[(p_{D^*}\cdot Q)^2 - Q^2 m_{D^*}^2\right] = m_{D^*}^2|\vec{p}_D|^2$ for $F = \pi$ and $2m_{D^*}^4|\vec{p}_D|^2$ for $F = \gamma$. Specifying the D^* polarization indices, one can write

$$|\mathcal{A}(D^* \to DF)|^2(m,n) = \Gamma(D^* \to DF)\frac{24\pi m_{D^*}^2}{|\vec{p}_D|^3}\,F_F(m,n), \tag{2.18}$$

with

$$F_F(m,n) = c_F\,[\epsilon(m)\cdot Q]\,[\epsilon(n)\cdot Q]^\dagger \tag{2.19}$$

and the constant $c_\pi = 1$ for $F=\pi$, and $c_\gamma = 1/(2m^2_{D^*})$ for $F=\gamma$. The (3×3) $F_F(m,n)$ matrices in (2.19) involve the angle θ_V:

$$F_\pi = \frac{|\vec{p}_D|^2}{2}\begin{pmatrix} \sin^2\theta_V & \sin^2\theta_V & \frac{1}{\sqrt{2}}\sin 2\theta_V \\ \sin^2\theta_V & \sin^2\theta_V & \frac{1}{\sqrt{2}}\sin 2\theta_V \\ \frac{1}{\sqrt{2}}\sin 2\theta_V & \frac{1}{\sqrt{2}}\sin 2\theta_V & 2\cos^2\theta_V \end{pmatrix} \tag{2.20}$$

$$F_\gamma = \frac{|\vec{p}_D|^2}{4}\begin{pmatrix} \frac{3+\cos 2\theta_V}{2} & -\sin^2\theta_V & -\frac{1}{\sqrt{2}}\sin 2\theta_V \\ -\sin^2\theta_V & \frac{3+\cos 2\theta_V}{2} & -\frac{1}{\sqrt{2}}\sin 2\theta_V \\ -\frac{1}{\sqrt{2}}\sin 2\theta_V & -\frac{1}{\sqrt{2}}\sin 2\theta_V & 2\sin^2\theta_V \end{pmatrix}. \tag{2.21}$$

Collecting the various terms in eq. (2.1) we obtain

$$\begin{aligned} |\mathcal{A}_{\rm TOT}(\bar{B}\to D^*(\to DF)\ell^-\bar{\nu}_\ell)|^2 &= G_F^2|V_{cb}|^2\frac{12\pi^2 m_{D^*}}{|\vec{p}_D|^3}\mathcal{B}(D^*\to DF)\delta(p^2_{D^*}-m^2_{D^*}) \\ &\times\left\{Tr\left[(\mathcal{H}^{\rm SM})^T\cdot F_F\right]+Tr\left[(\mathcal{H}^{\rm NP})^T\cdot F_F\right]+Tr\left[(\mathcal{H}^{\rm INT})^T\cdot F_F\right]\right\}, \end{aligned} \tag{2.22}$$

where the trace is carried out over the indices (m,n), ordered as $(1,2,3)=(+,-,0)$, and T meaning the transpose. The expression of the fully differential decay distribution can be worked out considering the four-body phase-space recalled in appendix A:

$$\begin{aligned} \frac{d^4\Gamma(\bar{B}\to D^*(\to DF)\ell^-\bar{\nu}_\ell)}{dq^2\,d\cos\theta\,d\phi\,d\cos\theta_V} &= \frac{3G_F^2|V_{cb}|^2\mathcal{B}(D^*\to DF)}{128(2\pi)^4 m_B^2}\frac{|\vec{p}_{D^*}|_{BRF}}{|\vec{p}_D|^2_{D^*RF}}\left(1-\frac{m_\ell^2}{q^2}\right) \\ &\times\left\{Tr\left[(\mathcal{H}^{\rm SM})^T\cdot F_F\right]+Tr\left[(\mathcal{H}^{\rm NP})^T\cdot F_F\right]+Tr\left[(\mathcal{H}^{\rm INT})^T\cdot F_F\right]\right\}. \end{aligned} \tag{2.23}$$

The hadronic matrix elements (2.4), (2.5) can be parametrized in terms of form factors. We use the definition

$$\begin{aligned} \langle D^*(p_{D^*},\epsilon)|\bar{c}\gamma_\mu(1-\gamma_5)b|\bar{B}(p_B)\rangle &= -\frac{2V(q^2)}{m_B+m_{D^*}}i\epsilon_{\mu\nu\alpha\beta}\epsilon^{*\nu}p_B^\alpha p_{D^*}^\beta \\ &-\left\{(m_B+m_{D^*})\left[\epsilon^*_\mu-\frac{(\epsilon^*\cdot q)}{q^2}q_\mu\right]A_1(q^2)\right. \\ &-\frac{(\epsilon^*\cdot q)}{m_B+m_{D^*}}\left[(p_B+p_{D^*})_\mu-\frac{m_B^2-m_{D^*}^2}{q^2}q_\mu\right]A_2(q^2) \\ &\left.+(\epsilon^*\cdot q)\frac{2m_{D^*}}{q^2}q_\mu A_0(q^2)\right\} \end{aligned} \tag{2.24}$$

(with the condition $A_0(0)=\dfrac{m_B+m_{D^*}}{2m_{D^*}}A_1(0)-\dfrac{m_B-m_{D^*}}{2m_{D^*}}A_2(0)$) and

$$\begin{aligned} \langle D^*(p_{D^*},\epsilon)|\bar{c}\sigma_{\mu\nu}(1-\gamma_5)b|\bar{B}(p_B)\rangle = {} & T_0(q^2)\frac{\epsilon^*\cdot q}{(m_B+m_{D^*})^2}\epsilon_{\mu\nu\alpha\beta}p_B^\alpha p_{D^*}^\beta + T_1(q^2)\epsilon_{\mu\nu\alpha\beta}p_B^\alpha\epsilon^{*\beta} \\ & +T_2(q^2)\epsilon_{\mu\nu\alpha\beta}p_{D^*}^\alpha\epsilon^{*\beta} \\ & +i\left[T_3(q^2)(\epsilon^*_\mu p_{B\nu}-\epsilon^*_\nu p_{B\mu})+T_4(q^2)(\epsilon^*_\mu p_{D^*\nu}-\epsilon^*_\nu p_{D^*\mu})\right. \\ & \left.+T_5(q^2)\frac{\epsilon^*\cdot q}{(m_B+m_{D^*})^2}(p_{B\mu}p_{D^*\nu}-p_{B\nu}p_{D^*\mu})\right]. \end{aligned} \tag{2.25}$$

JHEP06(2018)082

We also define $\tilde{T}_0 = T_0 - T_5$, $\tilde{T}_1 = T_1 + T_3$ and $\tilde{T}_2 = T_2 + T_4$. In appendix B we describe other matrix element parametrizations. In SM one can relate the helicity amplitudes for the D^* polarization states to the polarizations of the virtual $W(q, \bar{\epsilon})$. In the LRF one writes

$$\bar{\epsilon}_\pm = \frac{1}{\sqrt{2}}(0,1,\pm i,0)\,, \qquad \bar{\epsilon}_0 = (0,0,0,1)\,, \qquad \bar{\epsilon}_t = (1,0,0,0)\,. \tag{2.26}$$

This allows to define the amplitudes

$$\begin{aligned} H_m &= \bar{\epsilon}^{*\mu}_m \epsilon^{*\alpha}_m T_{\mu\alpha} && (m = 0, \pm) \\ H_t &= \bar{\epsilon}^{*\mu}_t \epsilon^{*\alpha}_0 T_{\mu\alpha} && (m = t)\,, \end{aligned} \tag{2.27}$$

which can be expressed in terms of the form factors in (2.24):

$$\begin{aligned} H_0 &= \frac{(m_B + m_{D^*})^2 (m_B^2 - m_{D^*}^2 - q^2) A_1(q^2) - \lambda(m_B^2,\, m_{D^*}^2,\, q^2) A_2(q^2)}{2 m_{D^*} (m_B + m_{D^*}) \sqrt{q^2}} \\ H_\pm &= \frac{(m_B + m_{D^*})^2 A_1(q^2) \mp \sqrt{\lambda(m_B^2,\, m_{D^*}^2,\, q^2)}\, V(q^2)}{m_B + m_{D^*}} \\ H_t &= -\frac{\sqrt{\lambda(m_B^2,\, m_{D^*}^2,\, q^2)}}{\sqrt{q^2}}\, A_0(q^2)\,. \end{aligned} \tag{2.28}$$

All the entries in $\mathcal{H}^{\rm SM}(m,n)$ can be written in terms of $H_\pm$, H_0 and H_t.

3 Angular decomposition of the fully differential decay distribution

The fully differential decay distribution for the chain process $\bar{B} \to D^*(\to DF)\ell^-\bar{\nu}_\ell$, with $F = \pi$ and $F = \gamma$, can be worked out in terms of the angles in figure 1. For $F = \pi$ it can be expressed as[3]

$$\begin{aligned} \frac{d^4\Gamma(\bar{B}\to D^*(\to D\pi)\ell^-\bar{\nu}_\ell)}{dq^2\, d\cos\theta\, d\phi\, d\cos\theta_V} = \mathcal{N}_\pi |\vec{p}_{D^*}| \left(1 - \frac{m_\ell^2}{q^2}\right)^2 \Big\{ & I_{1s}^\pi \sin^2\theta_V + I_{1c}^\pi \cos^2\theta_V \\ & + \left(I_{2s}^\pi \sin^2\theta_V + I_{2c}^\pi \cos^2\theta_V\right)\cos 2\theta \\ & + I_3^\pi \sin^2\theta_V \sin^2\theta \cos 2\phi + I_4^\pi \sin 2\theta_V \sin 2\theta \cos\phi \\ & + I_5^\pi \sin 2\theta_V \sin\theta \cos\phi + \left(I_{6s}^\pi \sin^2\theta_V + I_{6c}^\pi \cos^2\theta_V\right)\cos\theta \\ & + I_7^\pi \sin 2\theta_V \sin\theta \sin\phi \Big\}\,, \end{aligned} \tag{3.1}$$

with $\mathcal{N}_F = \dfrac{3G_F^2 |V_{cb}|^2 \mathcal{B}(D^* \to DF)}{128(2\pi)^4 m_B^2}$. For $F = \gamma$ we adopt the decomposition

$$\begin{aligned} \frac{d^4\Gamma(\bar{B}\to D^*(\to D\gamma)\ell^-\bar{\nu}_\ell)}{dq^2\, d\cos\theta\, d\phi\, d\cos\theta_V} = \mathcal{N}_\gamma |\vec{p}_{D^*}| \left(1 - \frac{m_\ell^2}{q^2}\right)^2 \Big\{ & I_{1s}^\gamma \sin^2\theta_V + I_{1c}^\gamma (3 + \cos 2\theta_V) \\ & + (I_{2s}^\gamma \sin^2\theta_V + I_{2c}^\gamma (3 + \cos 2\theta_V))\cos 2\theta \\ & + I_3^\gamma \sin^2\theta_V \sin^2\theta \cos 2\phi + I_4^\gamma \sin 2\theta_V \sin 2\theta \cos\phi \\ & + I_5^\gamma \sin 2\theta_V \sin\theta \cos\phi + (I_{6s}^\gamma \sin^2\theta_V + I_{6c}^\gamma (3 + \cos 2\theta_V))\cos\theta \\ & + I_7^\gamma \sin 2\theta_V \sin\theta \sin\phi \Big\}\,. \end{aligned} \tag{3.2}$$

[3] In principle, other two structures $I_8 \sin 2\theta_V \sin 2\theta \sin\phi + I_9 \sin^2\theta_V \sin^2\theta \sin 2\phi$ could be present in these decompositions. We do not include them, since they are absent in SM and in the NP model considered here.

In the Standard Model the coefficients of the angular terms are related to the helicity amplitudes (2.28):

$$
\begin{aligned}
I_{1s}^{\pi} &= \frac{1}{2}(H_+^2 + H_-^2)(m_\ell^2 + 3q^2)\,, & I_{1c}^{\pi} &= 2(2m_\ell^2 H_t^2 + H_0^2(m_\ell^2 + q^2))\,,\\
I_{2s}^{\pi} &= \frac{1}{2}(H_+^2 + H_-^2)(q^2 - m_\ell^2)\,, & I_{2c}^{\pi} &= 2H_0^2(m_\ell^2 - q^2)\,,\\
I_{3}^{\pi} &= 2H_+H_-(m_\ell^2 - q^2)\,, & I_{4}^{\pi} &= H_0(H_+ + H_-)(m_\ell^2 - q^2)\,,\\
I_{5}^{\pi} &= -2(H_+ + H_-)H_t m_\ell^2 - 2H_0(H_+ - H_-)q^2\,, & &\\
I_{6s}^{\pi} &= 2(H_+^2 - H_-^2)q^2\,, & I_{6c}^{\pi} &= -8H_0H_t m_\ell^2\,,\\
I_{7}^{\pi} &= 0\,,
\end{aligned}
\tag{3.3}
$$

and

$$
\begin{aligned}
I_{1s}^{\gamma} &= 2m_\ell^2 H_t^2 + H_0^2(m_\ell^2 + q^2)\,, & I_{1c}^{\gamma} &= \frac{1}{8}(H_+^2 + H_-^2)(m_\ell^2 + 3q^2)\,,\\
I_{2s}^{\gamma} &= H_0^2(m_\ell^2 - q^2)\,, & I_{2c}^{\gamma} &= \frac{1}{8}(H_+^2 + H_-^2)(q^2 - m_\ell^2)\,,\\
I_{3}^{\gamma} &= -H_+H_-(m_\ell^2 - q^2)\,, & I_{4}^{\gamma} &= -\frac{1}{2}H_0(H_+ + H_-)(m_\ell^2 - q^2)\,,\\
I_{5}^{\gamma} &= (H_+ + H_-)H_t m_\ell^2 + H_0(H_+ - H_-)q^2\,, & &\\
I_{6s}^{\gamma} &= -4H_0H_t m_\ell^2\,, & I_{6c}^{\gamma} &= \frac{1}{2}(H_+^2 - H_-^2)q^2\,,\\
I_{7}^{\gamma} &= 0\,.
\end{aligned}
\tag{3.4}
$$

Hence, the coefficients in $D\pi$ and $D\gamma$ angular distributions obey the relations, for all q^2,

$$
\frac{I_{1s}^{\pi}}{4I_{1c}^{\gamma}} = \frac{I_{1c}^{\pi}}{2I_{1s}^{\gamma}} = \frac{I_{2s}^{\pi}}{4I_{2c}^{\gamma}} = \frac{I_{2c}^{\pi}}{2I_{2s}^{\gamma}} = \frac{I_{6s}^{\pi}}{4I_{6c}^{\gamma}} = \frac{I_{6c}^{\pi}}{2I_{6s}^{\gamma}} = -\frac{I_{3}^{\pi}}{2I_{3}^{\gamma}} = -\frac{I_{4}^{\pi}}{2I_{4}^{\gamma}} = -\frac{I_{5}^{\pi}}{2I_{5}^{\gamma}} = 1\,. \tag{3.5}
$$

Integrated distributions are written in terms of the angular coefficients. In particular, the q^2 distributions read:

$$
\left.\frac{d\Gamma}{dq^2}\right|_{F=\pi} = \mathcal{N}_\pi |\vec{p}_{D^*}| \left(1 - \frac{m_\ell^2}{q^2}\right)^2 \frac{8}{9}\pi \left(6I_{1s}^{\pi} + 3I_{1c}^{\pi} - 2I_{2s}^{\pi} - I_{2c}^{\pi}\right)\,, \tag{3.6}
$$

$$
\left.\frac{d\Gamma}{dq^2}\right|_{F=\gamma} = \mathcal{N}_\gamma |\vec{p}_{D^*}| \left(1 - \frac{m_\ell^2}{q^2}\right)^2 \frac{16}{9}\pi \left(3I_{1s}^{\gamma} + 12I_{1c}^{\gamma} - I_{2s}^{\gamma} - 4I_{2c}^{\gamma}\right)\,. \tag{3.7}
$$

The angular coefficients encode information on the form factors, and vice-versa. Their fit from the experimental fully differential decay distribution allows to reconstruct the form factors, with a possible comparison of measurements to theory determinations. Considering

JHEP06(2018)082

the $D\pi$ mode one has

$$
\begin{aligned}
A_1(q^2) &= \frac{1}{4(m_B+m_{D^*})}\left\{\sqrt{\frac{4I^\pi_{1s}}{m_\ell^2+3q^2}-\frac{I^\pi_{6s}}{q^2}}+\sqrt{\frac{4I^\pi_{1s}}{m_\ell^2+3q^2}+\frac{I^\pi_{6s}}{q^2}}\right\},\\
A_2(q^2) &= \frac{(m_B+m_{D^*})}{4\lambda(m_B^2,\,m_{D^*}^2,\,q^2)}\left\{(m_B^2-m_{D^*}^2-q^2)\left[\sqrt{\frac{4I^\pi_{1s}}{m_\ell^2+3q^2}-\frac{I^\pi_{6s}}{q^2}}+\sqrt{\frac{4I^\pi_{1s}}{m_\ell^2+3q^2}+\frac{I^\pi_{6s}}{q^2}}\right]\right.\\
&\quad\left.-4\sqrt{2}m_{D^*}\sqrt{q^2}\sqrt{-\frac{I^\pi_{2c}}{q^2-m_\ell^2}}\right\},\\
V(q^2) &= \frac{(m_B+m_{D^*})}{4\lambda^{1/2}(m_B^2,\,m_{D^*}^2,\,q^2)}\left\{\sqrt{\frac{4I^\pi_{1s}}{m_\ell^2+3q^2}-\frac{I^\pi_{6s}}{q^2}}-\sqrt{\frac{4I^\pi_{1s}}{m_\ell^2+3q^2}+\frac{I^\pi_{6s}}{q^2}}\right\},\\
A_0(q^2) &= \frac{1}{2}\frac{\sqrt{q^2}}{\lambda^{1/2}(m_B^2,\,m_{D^*}^2,\,q^2)}\sqrt{\frac{(q^2-m_\ell^2)\,I^\pi_{1c}+(q^2+m_\ell^2)\,I^\pi_{2c}}{m_\ell^2(q^2-m_\ell^2)}}.
\end{aligned}
\tag{3.8}
$$

Analogously, from the $D\gamma$ mode one has

$$
\begin{aligned}
A_1(q^2) &= \frac{1}{2(m_B+m_{D^*})}\left\{\sqrt{\frac{4I^\gamma_{1c}}{m_\ell^2+3q^2}-\frac{I^\gamma_{6c}}{q^2}}+\sqrt{\frac{4I^\gamma_{1c}}{m_\ell^2+3q^2}+\frac{I^\gamma_{6c}}{q^2}}\right\},\\
A_2(q^2) &= \frac{(m_B+m_{D^*})}{2\lambda(m_B^2,\,m_{D^*}^2,\,q^2)}\left\{(m_B^2-m_{D^*}^2-q^2)\left[\sqrt{\frac{4I^\gamma_{1c}}{m_\ell^2+3q^2}-\frac{I^\gamma_{6c}}{q^2}}+\sqrt{\frac{4I^\gamma_{1c}}{m_\ell^2+3q^2}+\frac{I^\gamma_{6c}}{q^2}}\right]\right.\\
&\quad\left.-4m_{D^*}\sqrt{q^2}\sqrt{-\frac{I^\gamma_{2s}}{q^2-m_\ell^2}}\right\},\\
V(q^2) &= \frac{(m_B+m_{D^*})}{2\lambda^{1/2}(m_B^2,\,m_{D^*}^2,\,q^2)}\left\{\sqrt{\frac{4I^\gamma_{1c}}{m_\ell^2+3q^2}-\frac{I^\gamma_{6c}}{q^2}}-\sqrt{\frac{4I^\gamma_{1c}}{m_\ell^2+3q^2}+\frac{I^\gamma_{6c}}{q^2}}\right\},\\
A_0(q^2) &= \frac{1}{\sqrt{2}}\frac{\sqrt{q^2}}{\lambda^{1/2}(m_B^2,\,m_{D^*}^2,\,q^2)}\sqrt{\frac{(q^2-m_\ell^2)\,I^\gamma_{1s}+(q^2+m_\ell^2)\,I^\gamma_{2s}}{m_\ell^2(q^2-m_\ell^2)}}\,.
\end{aligned}
\tag{3.9}
$$

Such relations require precise signs for the angular coefficient functions and for a few of their combinations.

Considering the tensor operator in the effective Hamiltonian (2.2), the fully differential decay distribution can still be written as in eqs. (3.1), (3.2), with the coefficients I_i replaced by $I_i+|\epsilon_T|^2 I_i^{\rm NP}+2Re(\epsilon_T)I_i^{\rm INT}$ for $i=1,\dots 6$, and by $I_i+|\epsilon_T|^2 I_i^{\rm NP}+2Im(\epsilon_T)I_i^{\rm INT}$ for $i=7$. With the definitions

$$
\begin{aligned}
H_+^{\rm NP} &= \frac{1}{2\sqrt{q^2}}\left\{\left[m_B^2-m_{D^*}^2+\lambda^{1/2}(m_B^2,m_{D^*}^2,q^2)\right](\tilde{T}_1+\tilde{T}_2)+q^2(\tilde{T}_1-\tilde{T}_2)\right\}\\
H_-^{\rm NP} &= \frac{1}{2\sqrt{q^2}}\left\{\left[m_B^2-m_{D^*}^2-\lambda^{1/2}(m_B^2,m_{D^*}^2,q^2)\right](\tilde{T}_1+\tilde{T}_2)+q^2(\tilde{T}_1-\tilde{T}_2)\right\}\\
H_L^{\rm NP} &= 2\left\{\frac{\lambda(m_B^2,m_{D^*}^2,q^2)}{m_{D^*}(m_B+m_{D^*})^2}\,\tilde{T}_0+2\frac{m_B^2+m_{D^*}^2-q^2}{m_{D^*}}\,\tilde{T}_1+4m_{D^*}\,\tilde{T}_2\right\}
\end{aligned}
\tag{3.10}
$$

one has:

$$
\begin{aligned}
I_{1s}^{\mathrm{NP},\pi} &= 2[(H_+^{\mathrm{NP}})^2 + (H_-^{\mathrm{NP}})^2](3m_\ell^2 + q^2), & I_{1c}^{\mathrm{NP},\pi} &= \frac{1}{8}(q^2 + m_\ell^2)(H_L^{\mathrm{NP}})^2,\\
I_{2s}^{\mathrm{NP},\pi} &= 2[(H_+^{\mathrm{NP}})^2 + (H_-^{\mathrm{NP}})^2](m_\ell^2 - q^2), & I_{2c}^{\mathrm{NP},\pi} &= \frac{1}{8}(q^2 - m_\ell^2)(H_L^{\mathrm{NP}})^2,\\
I_{3}^{\mathrm{NP},\pi} &= 8H_+^{\mathrm{NP}}H_-^{\mathrm{NP}}(q^2 - m_\ell^2), & I_{4}^{\mathrm{NP},\pi} &= \frac{1}{2}(q^2 - m_\ell^2)H_L^{\mathrm{NP}}[H_+^{\mathrm{NP}} + H_-^{\mathrm{NP}}],\\
I_{5}^{\mathrm{NP},\pi} &= -m_\ell^2 H_L^{\mathrm{NP}}[H_+^{\mathrm{NP}} - H_-^{\mathrm{NP}}], & & \\
I_{6s}^{\mathrm{NP},\pi} &= 8m_\ell^2[(H_+^{\mathrm{NP}})^2 - (H_-^{\mathrm{NP}})^2], & I_{6c}^{\mathrm{NP},\pi} &= 0,\\
I_{7}^{\mathrm{NP},\pi} &= 0,
\end{aligned} \tag{3.11}
$$

and

$$
\begin{aligned}
I_{1s}^{\mathrm{NP},\gamma} &= \frac{1}{16}(H_L^{\mathrm{NP}})^2(q^2 + m_\ell^2), & I_{1c}^{\mathrm{NP},\gamma} &= \frac{1}{2}[(H_+^{\mathrm{NP}})^2 + (H_-^{\mathrm{NP}})^2](3m_\ell^2 + q^2),\\
I_{2s}^{\mathrm{NP},\gamma} &= \frac{1}{16}(q^2 - m_\ell^2)(H_L^{\mathrm{NP}})^2, & I_{2c}^{\mathrm{NP},\gamma} &= -\frac{1}{2}[(H_+^{\mathrm{NP}})^2 + (H_-^{\mathrm{NP}})^2](q^2 - m_\ell^2),\\
I_{3}^{\mathrm{NP},\gamma} &= -4H_+^{\mathrm{NP}}H_-^{\mathrm{NP}}(q^2 - m_\ell^2), & I_{4}^{\mathrm{NP},\gamma} &= -\frac{1}{4}(q^2 - m_\ell^2)H_L^{\mathrm{NP}}[H_+^{\mathrm{NP}} + H_-^{\mathrm{NP}}],\\
I_{5}^{\mathrm{NP},\gamma} &= \frac{1}{2}m_\ell^2 H_L^{\mathrm{NP}}[H_+^{\mathrm{NP}} - H_-^{\mathrm{NP}}], & & \\
I_{6s}^{\mathrm{NP},\gamma} &= 0, & I_{6c}^{\mathrm{NP},\gamma} &= 2m_\ell^2[(H_+^{\mathrm{NP}})^2 - (H_-^{\mathrm{NP}})^2],\\
I_{7}^{\mathrm{NP},\gamma} &= 0.
\end{aligned} \tag{3.12}
$$

The interference terms are given by

$$
\begin{aligned}
I_{1s}^{\mathrm{INT},\pi} &= -4\sqrt{q^2}\, m_\ell(H_+^{\mathrm{NP}}H_+ + H_-^{\mathrm{NP}}H_-), & I_{1c}^{\mathrm{INT},\pi} &= -\sqrt{q^2}\, m_\ell H_0 H_L^{\mathrm{NP}},\\
I_{2s}^{\mathrm{INT},\pi} &= 0, & I_{2c}^{\mathrm{INT},\pi} &= 0,\\
I_{3}^{\mathrm{INT},\pi} &= 0, & I_{4}^{\mathrm{INT},\pi} &= 0,\\
I_{5}^{\mathrm{INT},\pi} &= \frac{1}{4}\sqrt{q^2}m_\ell\left[H_L^{\mathrm{NP}}(H_+ - H_-) + 8H_0(H_+^{\mathrm{NP}} - H_-^{\mathrm{NP}}) + 8H_t(H_+^{\mathrm{NP}} + H_-^{\mathrm{NP}})\right], & &\\
I_{6s}^{\mathrm{INT},\pi} &= -4\sqrt{q^2}\, m_\ell(H_+^{\mathrm{NP}}H_+ - H_-^{\mathrm{NP}}H_-), & I_{6c}^{\mathrm{INT},\pi} &= \sqrt{q^2}\, m_\ell H_L^{\mathrm{NP}}H_t,\\
I_{7}^{\mathrm{INT},\pi} &= \frac{1}{4}\sqrt{q^2}m_\ell\left[H_L^{\mathrm{NP}}(H_+ + H_-) - 8H_0(H_+^{\mathrm{NP}} + H_-^{\mathrm{NP}}) - 8H_t(H_+^{\mathrm{NP}} - H_-^{\mathrm{NP}})\right],
\end{aligned} \tag{3.13}
$$

and

$$
\begin{aligned}
I_{1s}^{\mathrm{INT},\gamma} &= -\frac{1}{2}\sqrt{q^2}\, m_\ell H_0 H_L^{\mathrm{NP}}, & I_{1c}^{\mathrm{INT},\gamma} &= -m_\ell\sqrt{q^2}(H_+^{\mathrm{NP}}H_+ + H_-^{\mathrm{NP}}H_-),\\
I_{2s}^{\mathrm{INT},\gamma} &= 0, & I_{2c}^{\mathrm{INT},\gamma} &= 0,\\
I_{3}^{\mathrm{INT},\gamma} &= 0, & I_{4}^{\mathrm{INT},\gamma} &= 0,\\
I_{5}^{\mathrm{INT},\gamma} &= \frac{1}{8}\, m_\ell\sqrt{q^2}\left[-H_L^{\mathrm{NP}}(H_+ - H_-) - 8H_0(H_+^{\mathrm{NP}} - H_-^{\mathrm{NP}}) - 8H_t(H_+^{\mathrm{NP}} + H_-^{\mathrm{NP}})\right], & &\\
I_{6s}^{\mathrm{INT},\gamma} &= \frac{1}{2}\, m_\ell\sqrt{q^2}H_t H_L^{\mathrm{NP}}, & I_{6c}^{\mathrm{INT},\gamma} &= -\sqrt{q^2}\, m_\ell(H_+^{\mathrm{NP}}H_+ - H_-^{\mathrm{NP}}H_-),\\
I_{7}^{\mathrm{INT},\gamma} &= \frac{1}{8}\sqrt{q^2}m_\ell\left[-H_L^{\mathrm{NP}}(H_+ + H_-) + 8H_0(H_+^{\mathrm{NP}} + H_-^{\mathrm{NP}}) + 8H_t(H_+^{\mathrm{NP}} - H_-^{\mathrm{NP}})\right].
\end{aligned} \tag{3.14}
$$

The relations (3.5) continue to hold.

4 Standard Model: scrutinizing CLN vs BGL parametrization

Understanding the role of the form factor parametrization of the $B \to D^*$ hadronic matrix element is important before the formulation of any strategy to disentangle possible NP effects. The angular distributions can help identifying observables less sensitive to the form factor parametrization, hence more suitable to uncover deviations from SM. Observables displaying a pronounced dependence on such parametrization can help in studying the impact of form factors.

The parametrizations based on the heavy quark limit make use of the relations among the form factors in HQ, in particular the connection, at the leading order in the $1/m_Q$ expansion, of all the form factors to the single Isgur-Wise function $\xi(w)$, with $w = \frac{m_B^2+m_{D^*}^2-q^2}{2m_B m_{D^*}}$ the product of B and $D^{(*)}$ four-velocities. $\xi(w)$ is normalized to unity at zero recoil $w = 1$. In the CLN formulation the relations are improved including perturbative α_s and power $1/m_b$, $1/m_c$ corrections [16]. In terms of the function $h_{A1}(w)$ defined in appendix B, which coincides with $A_1(q^2)$ modulo a w-dependent coefficient, one can write

$$\begin{aligned} V(w) &= \frac{R_1(w)}{R^*} h_{A_1}(w) \\ A_1(w) &= \frac{w+1}{2} R^* h_{A_1}(w) \\ A_2(w) &= \frac{R_2(w)}{R^*} h_{A_1}(w) \\ A_0(w) &= \frac{R_0(w)}{R^*} h_{A_1}(w) \end{aligned} \tag{4.1}$$

with $R^* = \dfrac{2\sqrt{m_B m_{D^*}}}{m_B + m_{D^*}}$. In this approach, $h_{A_1}(w)$, $R_1(w)$, $R_2(w)$ and $R_0(w)$ are expanded for $w \to 1$, fixing the series coefficients using dispersive bounds [16]:

$$\begin{aligned} h_{A_1}(w) &= h_{A_1}(1) \left[1 - 8\rho^2 z + (53\rho^2 - 15)z^2 - (231\rho^2 - 91)z^3\right] \\ R_1(w) &= R_1(1) - 0.12(w-1) + 0.05(w-1)^2 \\ R_2(w) &= R_2(1) + 0.11(w-1) - 0.06(w-1)^2 \\ R_0(w) &= R_0(1) - 0.11(w-1) + 0.01(w-1)^2 \,, \end{aligned} \tag{4.2}$$

with the conformal variable z defined as $z = \dfrac{\sqrt{w+1}-\sqrt{2}}{\sqrt{w+1}+\sqrt{2}}$. In the HQ limit the predictions

$$R_1^{HQ}(1) = 1.27 \,, \qquad R_2^{HQ}(1) = 0.80 \,, \qquad R_0^{HQ}(1) = 1.25 \tag{4.3}$$

are obtained [12, 16]. However, in the experimental analyses making use of this parametrization, not only the slope ρ^2, but also the ratios $R_1(1)$ and $R_2(1)$ are fitted parameters, while $h_{A_1}(1)$ is taken from lattice QCD calculations. $R_0(1)$ is involved in the case of τ lepton, and no experimental result is available. The parameters fitted by Belle Collaboration [17], that we use in our analysis, are collected in table 1. We use the last relation in (4.1), together with the expressions (B.4) in appendix B, to obtain $R_0(1)$.

JHEP06(2018)082

$\lvert V_{cb}\rvert \times 10^3$	ρ^2	$R_1(1)$	$R_2(1)$
37.4 ± 1.3	1.03 ± 0.13	1.38 ± 0.07	0.87 ± 0.10

Table 1. CLN parameters fitted by Belle Collaboration [17].

In the BGL formulation, recalled in appendix B, the form factors are expressed as functions of the conformal variable z. After having included outer functions [45] and subtracted the contribution of $b\bar{c}$ states, the form factors are expressed as power series of z, with the coefficients determined by a fit to the experimental data [18–20]. The number of parameters for each form factor is larger than in CLN; on the other hand, no information from the HQ limit is used. In our analysis we use the parameters in [21], obtained fitting the same data set in [17], in the case where input from light-cone QCD sum rules is included. In the absence of results from the fits, also in this case we use the HQ relations to obtain R_0, as in [10].

A point emphasized in [10, 21, 22] is that, although the Belle data in [17] can be well reproduced using both parametrizations, the high q^2 bins are better described by BGL, with a value of $|V_{cb}|$ larger than using CLN and closer to the inclusive $|V_{cb}|$ determination. Moreover, these Belle data seem to suggest deviations from HQ symmetry and tensions with preliminary lattice results for the ratio R_1 [46], as noticed comparing the data to fits using BGL or various versions of CLN parametrization [47].

In principle, the angular coefficient functions inferred from the fully differential distribution can be used to reconstruct the form factors. In particular, for the ratios $R_1(w)$ and $R_2(w)$ one has:

$$R_1(w) = \frac{8q^2 m_B m_{D^*}(1+w)}{(m_\ell^2+3q^2)\lambda^{1/2}(m_B^2, m_{D^*}^2, q^2)}\frac{1}{I_{6s}^\pi}\left[\sqrt{(I_{1s}^\pi)^2 - \left(\frac{m_\ell^2+3q^2}{q^2}\right)^2\frac{(I_{6s}^\pi)^2}{16}} - I_{1s}^\pi\right], \quad (4.4)$$

$$R_2(w) = \frac{2m_B m_{D^*}(1+w)}{\lambda(m_B^2, m_{D^*}^2, q^2)}\Bigg[(m_B^2 - q^2 - m_{D^*}^2) \quad (4.5)$$

$$+ 2\sqrt{2} m_{D^*} q^2 \sqrt{-\frac{q^2}{q^2-m_\ell^2} I_{2c}^\pi}\,\frac{1}{I_{6s}^\pi}\left(\sqrt{\frac{4I_{1s}^\pi}{m_\ell^2+3q^2} - \frac{I_{6s}^\pi}{q^2}} - \sqrt{\frac{4I_{1s}^\pi}{m_\ell^2+3q^2} + \frac{I_{6s}^\pi}{q^2}}\right)\Bigg].$$

This is interesting, since a difference between the CLN and BGL parametrizations emerges in these ratios [10, 21, 47].

We now investigate the angular coefficient functions obtained with CLN and BGL, using their respective set of parameters. The results are collected in figure 2. We use as an input the lattice QCD value $h_{A_1}(1) = 0.906 \pm 0.013$ [48] times the ew correction factor $\eta_W = 1.0066$ [49, 50]. We also show the results obtained in the HQ limit using eq. (4.3).

The functions I_{1s}^π, I_{2s}^π, I_3^π, I_4^π, and I_{1c}^γ, I_{2c}^γ, I_3^γ, I_4^γ are largely insensitive to the form factor parametrization. On the contrary, I_{1c}^π, I_{2c}^π, I_{6s}^π, and I_{1s}^γ, I_{2s}^γ, I_{6c}^γ are more dependent. The coefficients I_{6c}^π, I_{6s}^γ are proportional to the lepton mass, hence they are small compared to the others for $\ell = \mu$. The indication is that the first set of coefficients is more suitable to pin down deviations from SM. In particular, $I_7^{\pi(\gamma)}$ vanishes in SM, therefore it is able

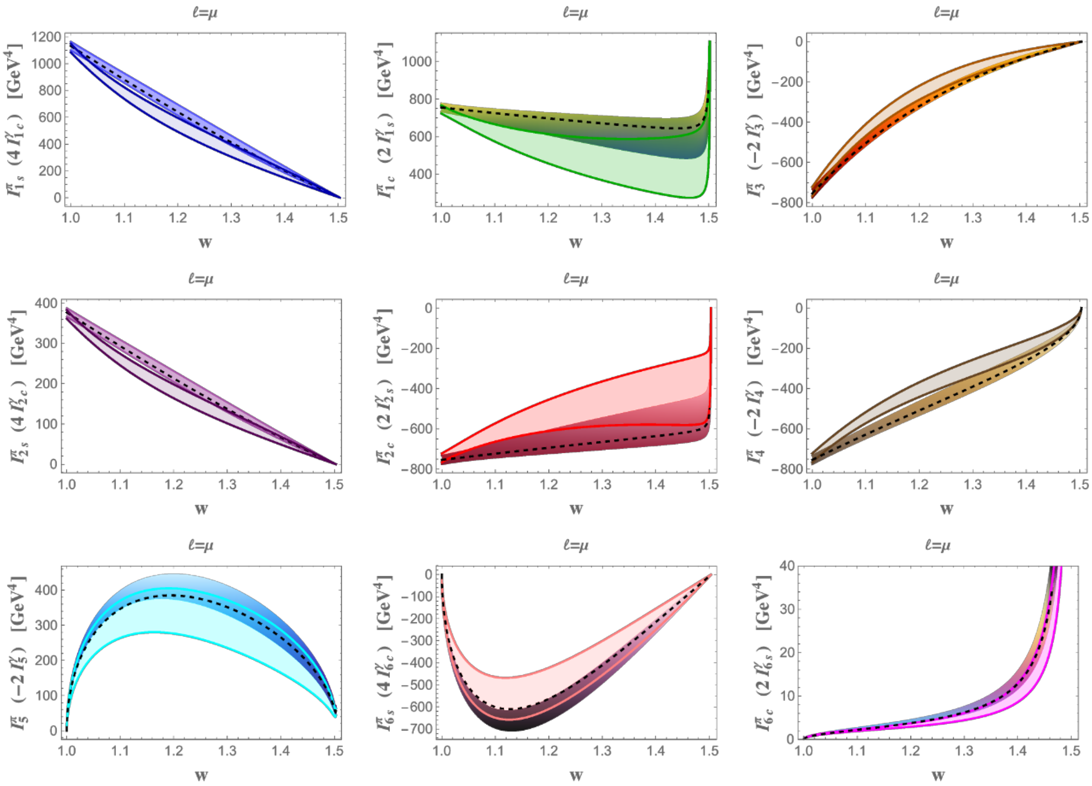

Figure 2. Angular coefficients in the fully differential decay distribution eq. (3.1) for $\ell = \mu$ in SM. The coefficients in (3.2) are obtained using the relations (3.5). The darker regions correspond to the CLN parametrization with parameters in table 1, the lighter regions to the BGL parametrization described in appendix B. The dashed lines are the HQ predictions.

to signal a NP effect: indeed, in the model with the tensor operator $\mathrm{Im}(\epsilon_T^\ell)$ can be non-vanishing, as well as $I_7^{\pi(\gamma)}$.

The second set of angular coefficient functions can be used to better evaluate the form factor parametrization. The results in BGL display larger uncertainties, and are systematically larger (smaller) than in CLN in I_{2c}^π, I_{6s}^π (I_{1c}^π, I_5^π). An overlap region spanned by the two parametrizations always exists, and the HQ result is closer to the CLN outcome, sometimes at the limits. An analogous trend is found for the $\ell = \tau$ mode, in the angular coefficient functions displayed in figure 3. Comparing I_{1c}^π and I_{2c}^π for $\ell = \mu$ and τ, one finds that the uncertainties are smaller in the case of the heavier lepton. Due to the difficulties discussed in the Introduction, the possibility of accessing the various I_i in the case of τ is very challenging. In particular, the reconstruction of the angle θ is not possible when the τ is reconstructed in decays to final states with multiple neutrinos. However, the reconstruction in visible 3-prong decays opens new interesting perspectives from this point of view, although with the caveat concerning the control of the $\pi^+\pi^+\pi^-\pi^0$ contribution discussed in the Introduction. Moreover, a set of integrated observables can be considered, with particular attention of those depending on the angle θ_V.

The complementarity of the modes with D^* decaying to $D\pi$ or to $D\gamma$ emerges from figures 4 and 5, obtained using the CLN parametrization. For $F = \pi$ the events are mainly

JHEP06(2018)082

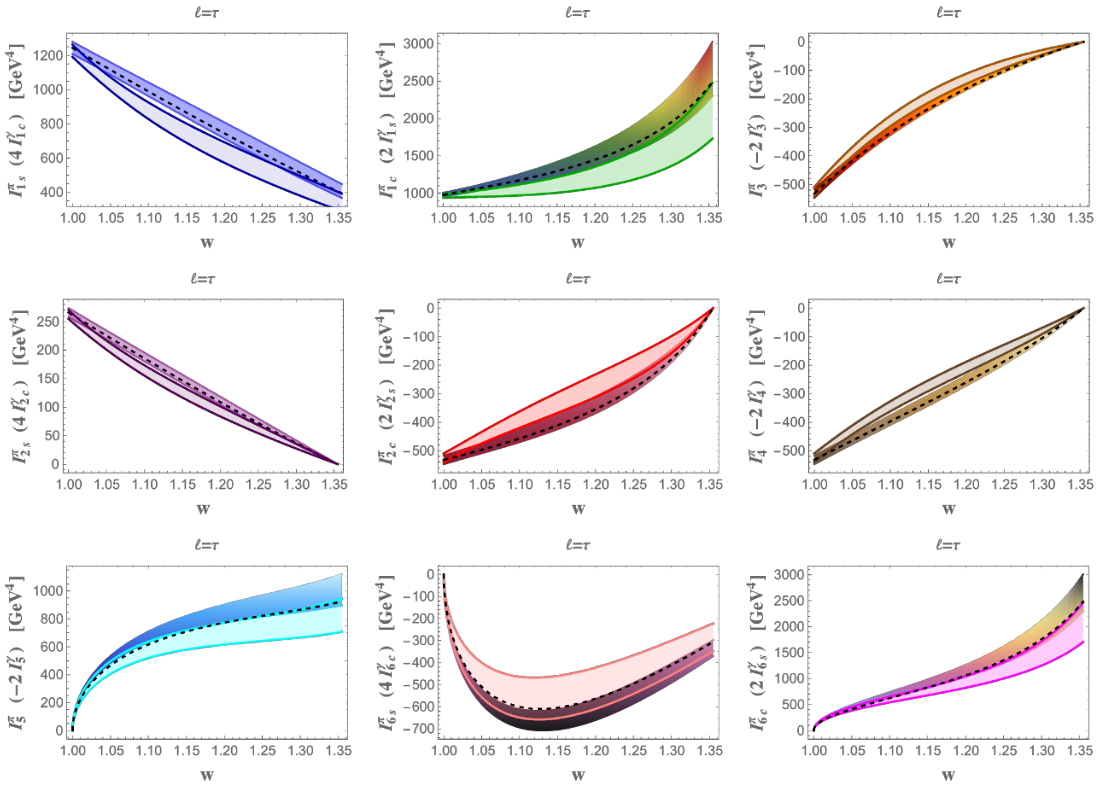

Figure 3. Angular coefficients in the fully differential decay distribution eq. (3.1) for $\ell = \tau$ in SM. The coefficients in (3.2) are obtained using (3.5). Color code as in figure 2.

at the limits of the $\cos\theta_V$ region, as shown both by the density plots in figure 4 and by the projections in figure 5. In the case of the photon, the most populated region is for $\cos\theta_V \simeq 0$. This should be taken into account in the analysis of $B_s \to D_s^{*+}\ell^-\bar{\nu}$, where the final state is dominated by the $D_s\gamma$ mode.

5 Angular coefficient functions in the NP model

In the case of the effective Hamiltonian with the tensor operator the angular coefficient functions are modified. To discuss the changes with respect to SM we need to fix a range for the couplings ϵ_T^μ and ϵ_T^τ. In [24] ϵ_T^τ was constrained by $R(D)$ and $R(D^*)$, assuming $\epsilon_T^\mu = \epsilon_T^e = 0$. In [23] the latter assumption was relaxed, $\epsilon_T^\mu \neq 0$ and $\epsilon_T^e \neq 0$, to reproduce $\bar{B} \to X_c\ell^-\bar{\nu}_\ell$ and $\bar{B} \to D^{(*)}\ell^-\bar{\nu}_\ell$ data in a common range of $|V_{cb}|$. We now consider these constraints, but since the ranges for ϵ_T^μ and ϵ_T^e turn out to be almost coincident, we only distinguish ϵ_T^μ and ϵ_T^τ. We adopt the CLN parametrization, employing the HQ relations (including $\mathcal{O}(\alpha_s)$ and $\mathcal{O}(1/m_Q)$ corrections [12], as reported in appendix B) to determine the form factors T_i in (2.25), since the BGL parametrization for such functions has not been developed.

We use the range of values of ϵ_T^μ selected in [23], restricted to reproduce $|V_{cb}|$ obtained by the Belle's fit in table 1 (within 2σ). In this range we compute $R(D)$ and $R(D^*)$

JHEP06(2018)082

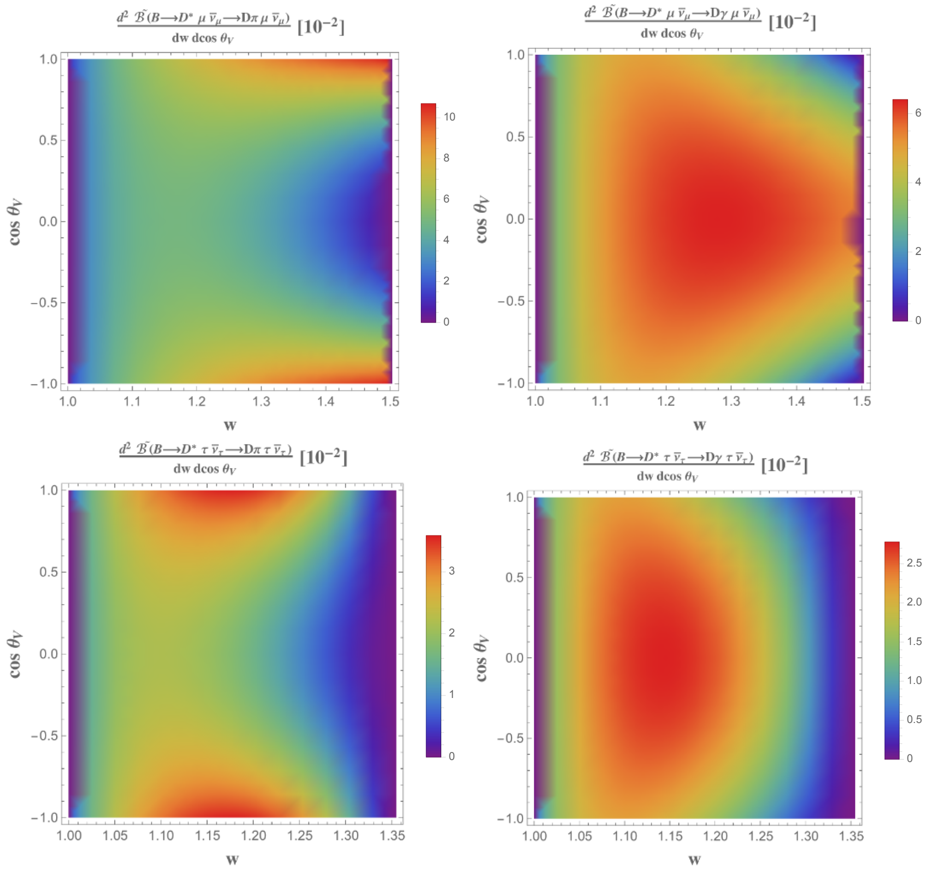

Figure 4. SM scatter plots of the double differential distributions in w and $\cos\theta_V$, with $\tilde{\mathcal{B}} = \mathcal{B}/\mathcal{B}(D^* \to DF)$, using the CLN parametrization. The upper and lower plots refer to $\ell = \mu$ and $\ell = \tau$ modes, respectively, the left and right column to $F = \pi$ and $F = \gamma$.

using the averages in eq. (1.1) at 1σ as constraints. For $R(D)$ we use lattice QCD form factors [51]. The obtained ranges for ϵ_T^μ and ϵ_T^τ are displayed in figure 6. The regions can be restricted imposing $\chi^2 = \left(\frac{R(D)-R(D)^{\rm exp}}{\Delta R(D)^{\rm exp}}\right)^2 + \left(\frac{R(D^*)-R(D^*)^{\rm exp}}{\Delta R(D^*)^{\rm exp}}\right)^2 \leq 1.0$. In this region we select the point corresponding to the minimum $|\tilde\epsilon_T^\mu|$, the black dot in figure 6, together with the corresponding value for ϵ_T^τ, with numerical values $(\mathrm{Re}(\tilde\epsilon_T^\mu), \mathrm{Im}(\tilde\epsilon_T^\mu)) = (0.115, -0.005)$ and $(\mathrm{Re}(\tilde\epsilon_T^\tau), \mathrm{Im}(\tilde\epsilon_T^\tau)) = (-0.067, 0)$. This is a benchmark point used to describe the sensitivity of the angular observables and the pattern of correlated deviations from SM in this scenario. In correspondence to this value, the fraction of longitudinally polarized D^* measured by Belle in [52] is reproduced, considering the various uncertainties, while the fraction of tranversely polarized D^* in the maximum recoil region turns out to deviate by more than 2σ in the last two bins of w. Indeed, this distribution is found to be SM-like: in SM for massless leptons the D^* is fully longitudinally polarized at $q^2 = 0$. Compatibility with data in this kinematical region would be obtained for $\mathrm{Re}(\epsilon_T^\mu) \leq 0.05$, in agreement with the findings in [34]. However, the purpose of our analysis is not to obtain the best fit of the NP coupling, a task deferred to different studies based on the full knowledge of the

JHEP06(2018)082

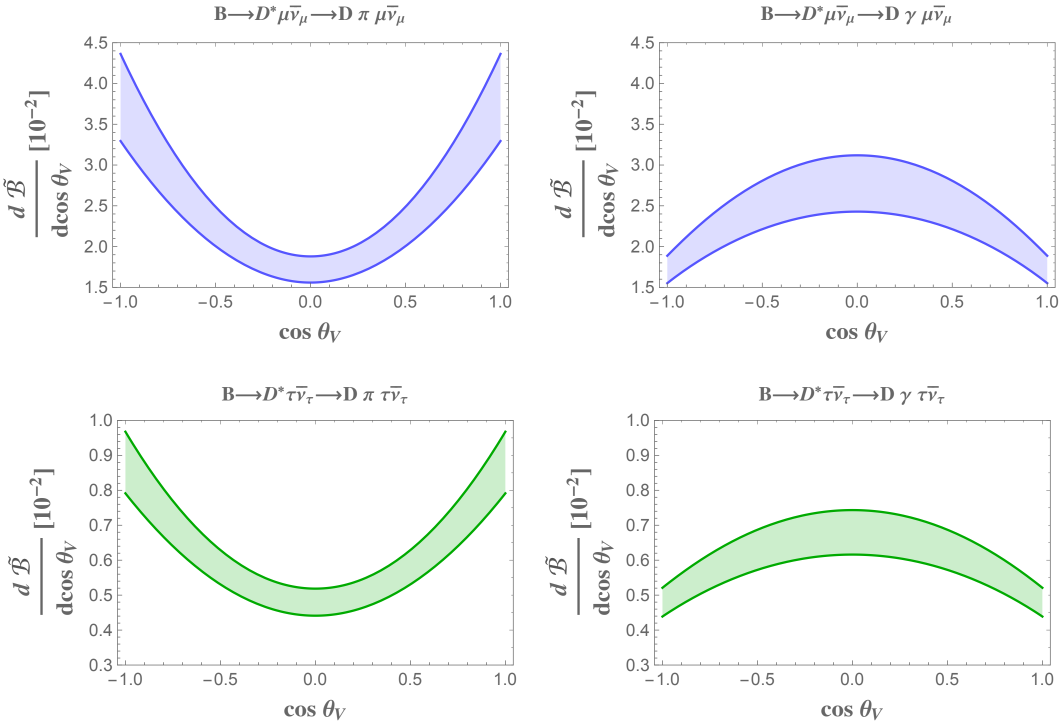

Figure 5. SM distributions in $\cos\theta_V$ using CLN, with $\tilde{\mathcal{B}} = \mathcal{B}/\mathcal{B}(D^* \to DF)$. The upper and lower plots refer to $\ell = \mu$ and $\ell = \tau$, respectively, the left and right column to $F = \pi$ and $F = \gamma$.

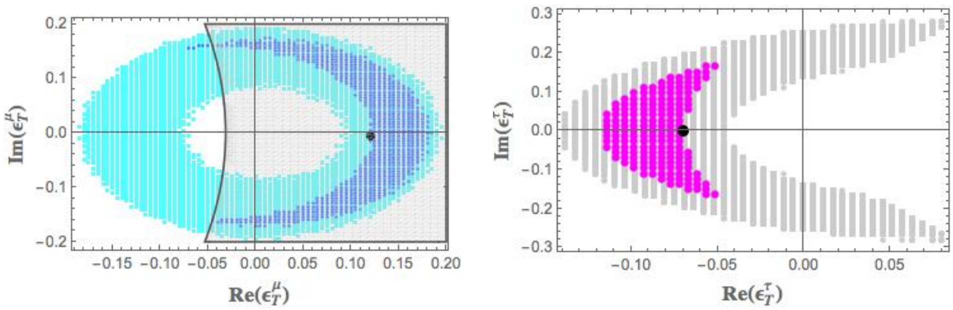

Figure 6. Parameter space of ϵ_T^μ (left) and ϵ_T^τ (right), determined using $R(D)$ and $R(D^*)$ in (1.1) (lighter regions). The darker regions correspond to $\chi^2 < 1.0$. In ϵ_T^μ the shaded gray region results using the Belle measurement of $R_{e\mu}$ [17]. The black dots are the values $\tilde{\epsilon}_T^\ell$ defined in the text, used as benchmark points.

data sets with their systematics, but to provide the overview on how the various observables coherently deviate from SM in this scenario. It should be remarked that in the selected parameter region, for $\epsilon_T^\mu = \epsilon_T^e$, the ratio $R_{e\mu} = \dfrac{\mathcal{B}(\bar{B}^0 \to D^{*+} e^- \bar{\nu}_e)}{\mathcal{B}(\bar{B}^0 \to D^{*+} \mu^- \bar{\nu}_\mu)} = 1.04 \pm 0.05 \pm 0.01$ [17] is reproduced: in figure 6, the shaded gray region is constrained by $R_{e\mu}$.

We compute the angular coefficients I_i using the parameters ϵ_T^μ, ϵ_T^τ in the low χ^2 region in figure 6, with the results shown in figures 7 and 8 for $\ell = \mu$ and $\ell = \tau$. Comparing the results in SM, the impact of NP is to modify the size of the coefficients, in several

JHEP06(2018)082

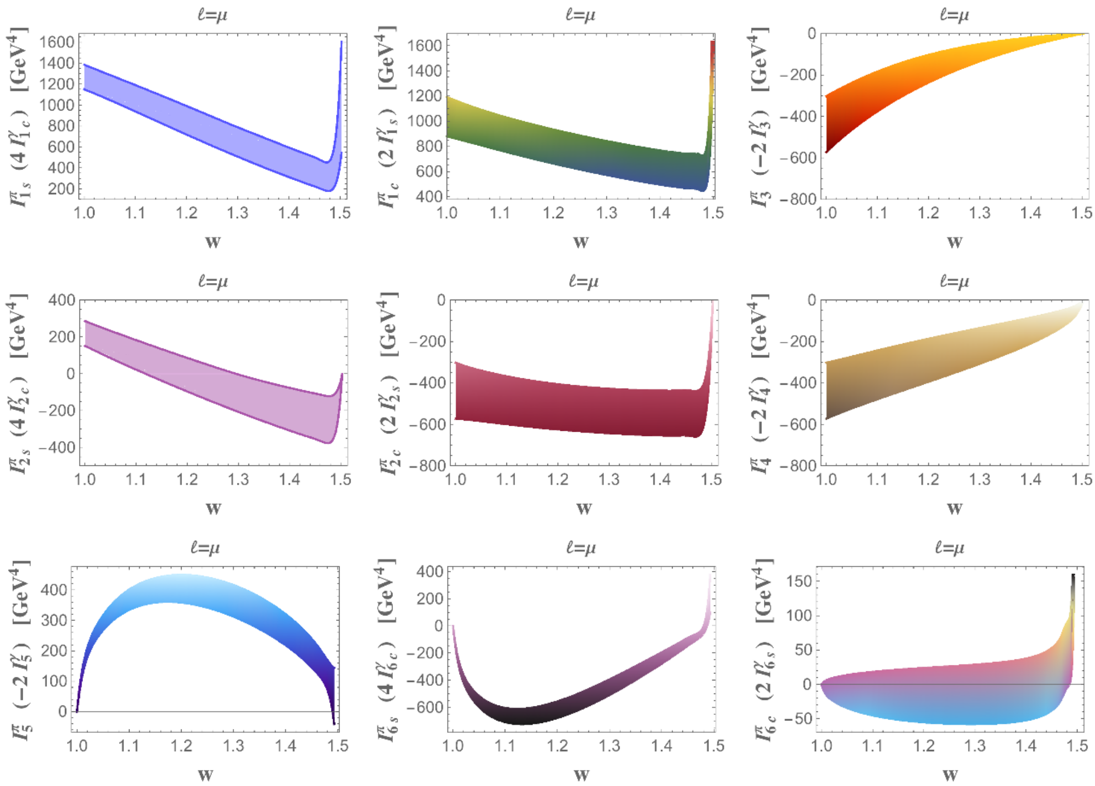

Figure 7. Angular coefficients in the fully differential decay distribution eq. (3.1) for $\ell = \mu$, with the tensor operator in the effective Hamiltonian and coupling ϵ_T^{μ} in the low χ^2 region displayed in figure 6.

cases mainly near the maximum recoil point $w \to w_{\rm max}$, as noticed in [34]. I_{2s}^{π} (I_{2c}^{γ}), always positive in SM, has a zero in NP. I_7 is displayed in figure 9; it is proportional to the lepton mass, hence it is small in the muon case, but it can be different from zero if ϵ_T^{ℓ} has non-zero imaginary part.

6 Scrutinizing deviations from SM

Starting from the set of angular coefficient functions, several observables can be constructed to scrutinize SM and possible anomalies. A few observables are independent of the D^* decay mode.

- The q^2*-dependent forward-backward (FB) lepton asymmetry* is defined as

$$A_{\rm FB}(q^2) = \left[\int_0^1 d\cos\theta\, \frac{d^2\Gamma}{dq^2 d\cos\theta} - \int_{-1}^0 d\cos\theta\, \frac{d^2\Gamma}{dq^2 d\cos\theta}\right] \Big/ \frac{d\Gamma}{dq^2}\,. \tag{6.1}$$

It can be expressed in terms of the coefficient functions:

$$A_{\rm FB}(q^2) = \frac{3(I_{6c}^{\pi} + 2I_{6s}^{\pi})}{6I_{1c}^{\pi} + 12I_{1s}^{\pi} - 2I_{2c}^{\pi} - 4I_{2s}^{\pi}} = \frac{3(I_{6s}^{\gamma} + 4I_{6c}^{\gamma})}{6I_{1s}^{\gamma} + 24I_{1c}^{\gamma} - 2I_{2s}^{\gamma} - 8I_{2c}^{\gamma}}\,, \tag{6.2}$$

JHEP06(2018)082

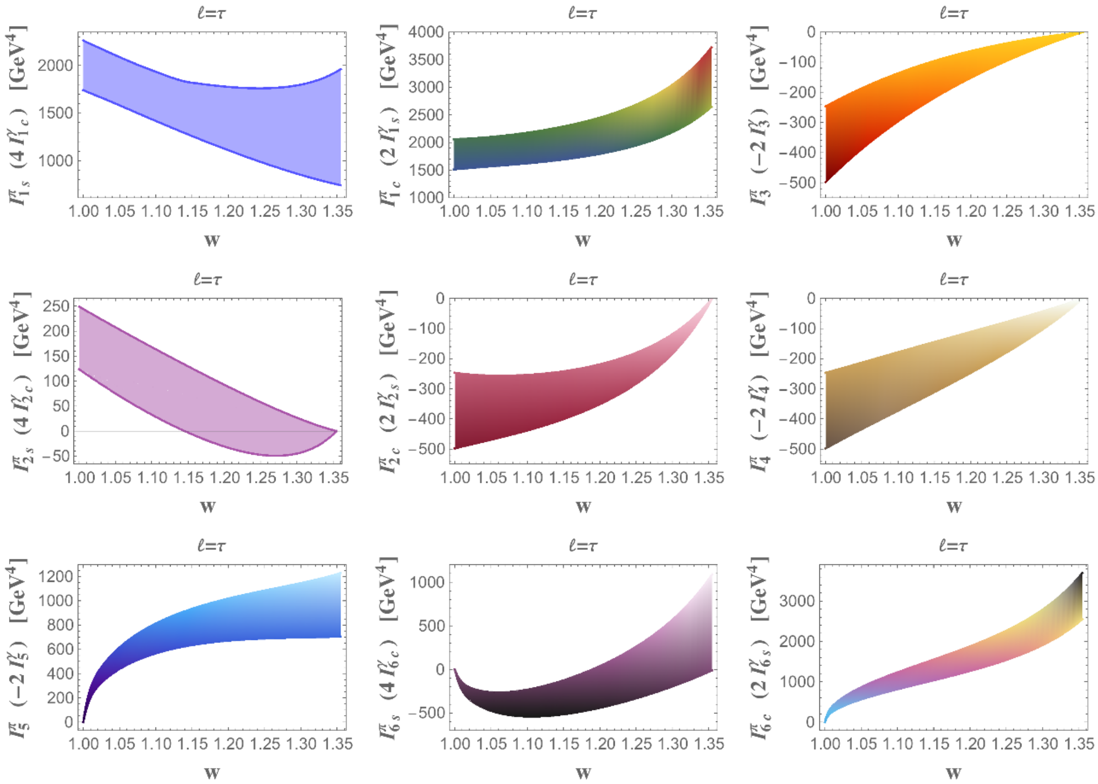

Figure 8. Angular coefficients in the fully differential decay distribution eq. (3.1) for $\ell = \tau$, with the tensor operator in the effective Hamiltonian and coupling ϵ_T^τ in the low χ^2 region displayed in figure 6.

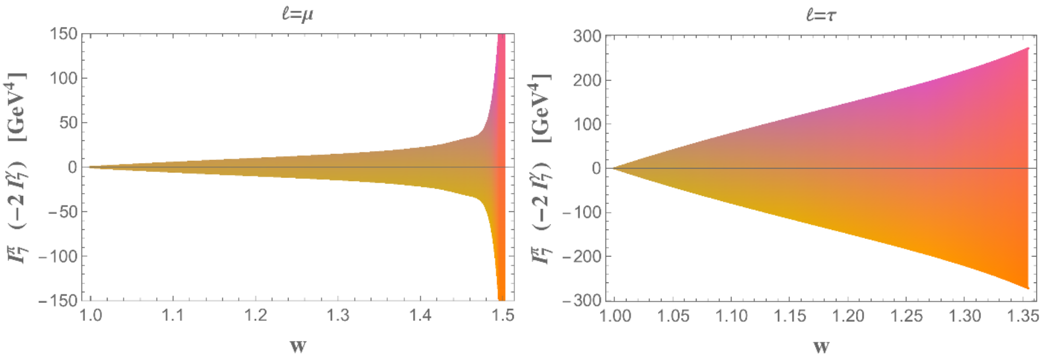

Figure 9. Coefficient I_7 in eq. (3.1) for $\ell = \mu$ and (left), and $\ell = \tau$ (right). The coefficients ϵ_T^μ and ϵ_T^τ are varied in the low χ^2 region displayed in figure 6. I_7 does not vanish when the tensor operator is included in the effective Hamiltonian.

JHEP06(2018)082

and in SM in terms of the helicity amplitudes

$$A_{\rm FB}(q^2)|_{\rm SM} = \frac{3q^2\left(H_+^2 - H_-^2\right) - 6m_\ell^2 H_0 H_t}{2m_\ell^2\left(H_0^2 + 3H_t^2 + H_+^2 + H_-^2\right) + 4q^2\left(H_0^2 + H_+^2 + H_-^2\right)}\,. \tag{6.3}$$

- The *transverse forward-backward (TFB) asymmetry* is the FB asymmetry for transversely polarized D^*. In SM it is expressed in terms of the helicity amplitudes

$$A^T_{\rm FB}(q^2)|_{\rm SM} = \frac{3q^2\left(H_+^2 - H_-^2\right)}{2(m_\ell^2 + 2q^2)\left(H_+^2 + H_-^2\right)}\,. \tag{6.4}$$

  $A^T_{\rm FB}$ only depends on the form factor ratio R_1, hence it is useful to check the HQ prediction for such a quantity [53].

- D^* *polarization asymmetry.* Defining the distributions $d\Gamma_{L(T)}/dq^2$ for longitudinally (L) and transversely (T) polarized D^*, a polarization asymmetry can be defined:

$$\frac{dA^{D^*}_{\rm pol}(q^2)}{dq^2} = 2\frac{d\Gamma_L}{dq^2}\Big/\frac{d\Gamma_T}{dq^2} - 1\,. \tag{6.5}$$

  A combination regular at $w \to w_{\rm max}$ is

$$\tilde{A}^{D^*}_{\rm pol}(q^2) = \frac{\dfrac{dA^{D^*}_{\rm pol}(q^2)}{dq^2}}{1 + \dfrac{dA^{D^*}_{\rm pol}(q^2)}{dq^2}}\,. \tag{6.6}$$

  In SM this quantity is expressed in terms of the helicity amplitudes:

$$\tilde{A}^{D^*}_{\rm pol}(q^2)|_{\rm SM} = 1 - \frac{(m_\ell^2 + 2q^2)\left(H_+^2 + H_-^2\right)}{6m_\ell^2 H_t^2 + 2(m_\ell^2 + 2q^2)H_0^2}\,. \tag{6.7}$$

In figure 10 we depict the SM results for these observables and the NP ones obtained at the benchmark point $\tilde{\epsilon}^\mu_T$ and $\tilde{\epsilon}^\tau_T$. The SM results are systematically modified in NP; in particular, a zero appears in $A_{\rm FB}(w)$ when $\ell = \tau$ [24]. $\tilde{A}^{D^*}_{\rm pol}$ shows a high sensitivity to the tensor structure for $w \to w_{\rm max}$, in particular in the case $\ell = \mu$, as noticed in [34], since in SM, for $m_\ell \to 0$, D^* is fully longitudinally polarized at this kinematical point.

An observable different when the final state involves a pion $F = \pi$ or a photon $F = \gamma$ is the

- $\cos\theta_V$*-dependent forward-backward asymmetry*, defined as

$$A_{\rm FB}(cos\theta_V) = \frac{\left[\int_0^1 dcos\,\theta\,\dfrac{d^2\Gamma}{dcos\theta_V dcos\,\theta} - \displaystyle\int_{-1}^0 dcos\,\theta\,\dfrac{d^2\Gamma}{dcos\theta_V dcos\,\theta}\right]}{\dfrac{d\Gamma}{dcos\theta_V}}\,. \tag{6.8}$$

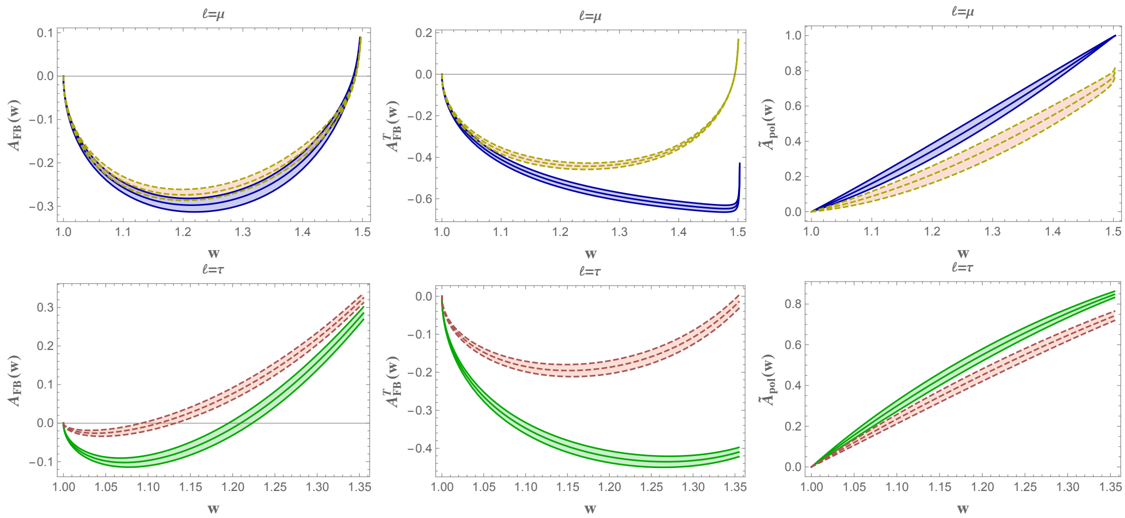

Figure 10. Observables defined in eq. (6.1) (left column), (6.4) (middle) and (6.6) (right). The upper and lower plots refer to $\ell = \mu$ and $\ell = \tau$, respectively. The solid curves correspond to SM, the dashed ones to NP at the benchmark point $\tilde{\epsilon}_T^\ell$.

Figure 11 shows the result in SM compared to NP for $\tilde{\epsilon}_T^\ell$. The deviation from SM is largest for $\cos\theta_V \simeq 0$ in the case of pion, and for $\cos\theta_V \simeq \pm 1$ when $F = \gamma$.

The sensitivity of the angular distributions to the D^* polarization can be studied considering the triple differential distributions obtained from (3.1) and (3.2) after integration in the angle ϕ. When D^* is longitudinally polarized one has

$$\frac{d^3\Gamma_L}{dq^2 d\cos\theta_V d\cos\theta}\bigg|_{F=\pi} = \mathcal{N}_\pi |\vec{p}_{D^*}| \left(1 - \frac{m_\ell^2}{q^2}\right)^2 2\pi \left[I_{1c}^\pi + I_{2c}^\pi \cos 2\theta + I_{6c}^\pi \cos\theta\right] \cos\theta_V^2 \tag{6.9}$$

$$\frac{d^3\Gamma_L}{dq^2 d\cos\theta_V d\cos\theta}\bigg|_{F=\gamma} = \mathcal{N}_\gamma |\vec{p}_{D^*}| \left(1 - \frac{m_\ell^2}{q^2}\right)^2 2\pi \left[I_{1s}^\gamma + I_{2s}^\gamma \cos 2\theta + I_{6s}^\gamma \cos\theta\right] \sin\theta_V^2, \tag{6.10}$$

and for transversely polarized D^* (summing over the two transverse polarizations)

$$\frac{d^3\Gamma_T}{dq^2 d\cos\theta_V d\cos\theta}\bigg|_{F=\pi} = \mathcal{N}_\pi |\vec{p}_{D^*}| \left(1 - \frac{m_\ell^2}{q^2}\right)^2 2\pi \left[I_{1s}^\pi + I_{2s}^\pi \cos 2\theta + I_{6s}^\pi \cos\theta\right] \sin\theta_V^2 \tag{6.11}$$

$$\frac{d^3\Gamma_T}{dq^2 d\cos\theta_V d\cos\theta}\bigg|_{F=\gamma} = \mathcal{N}_\gamma |\vec{p}_{D^*}| \left(1 - \frac{m_\ell^2}{q^2}\right)^2 2\pi \left[I_{1c}^\gamma + I_{2c}^\gamma \cos 2\theta + I_{6c}^\gamma \cos\theta\right] (3 + \cos 2\theta_V). \tag{6.12}$$

Double differential D^* polarization fractions can be defined:

$$F_L(\theta,\, \theta_V) = \frac{1}{\Gamma(\bar{B} \to D^*(DF)\ell^-\bar{\nu}_\ell)} \int_{q^2_{\rm min}}^{q^2_{\rm max}} dq^2 \frac{d^3\Gamma_L}{dq^2 d\cos\theta_V d\cos\theta} \tag{6.13}$$

$$F_T(\theta,\, \theta_V) = \frac{1}{\Gamma(\bar{B} \to D^*(DF)\ell^-\bar{\nu}_\ell)} \int_{q^2_{\rm min}}^{q^2_{\rm max}} dq^2 \frac{d^3\Gamma_T}{dq^2 d\cos\theta_V d\cos\theta}\,. \tag{6.14}$$

These quantities keep the same angular dependence as in (6.9)–(6.12). In particular, they are simmetric under $\cos\theta_V \to -\cos\theta_V$, but they have no definite behavior when $\cos\theta \to$

JHEP06(2018)082

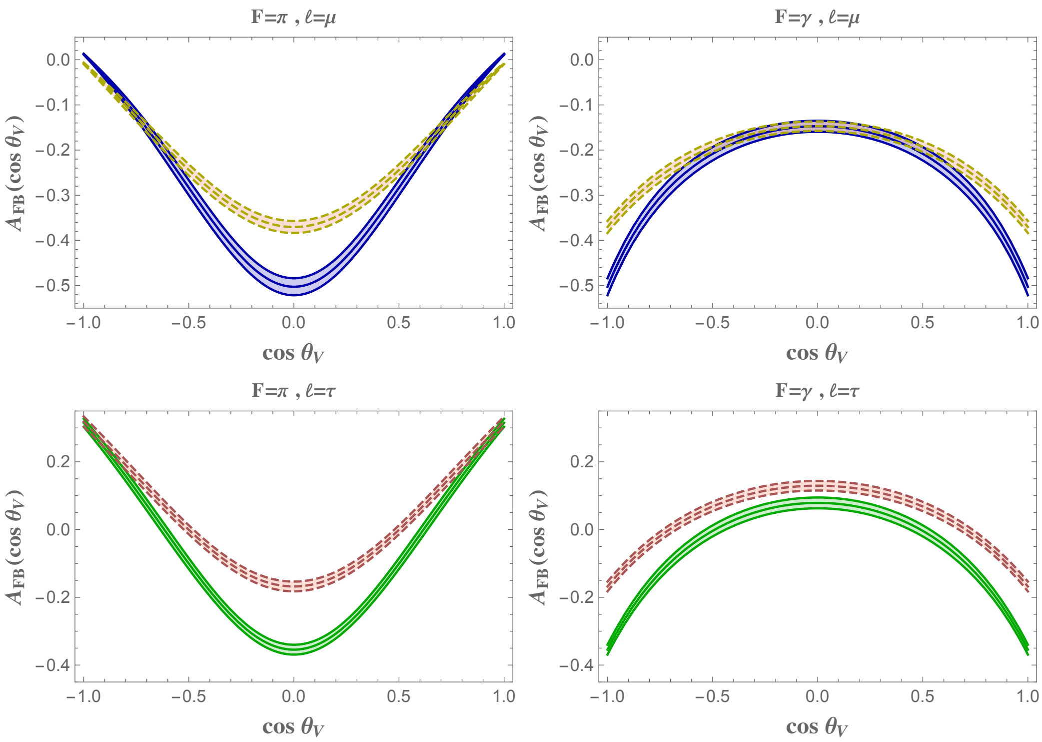

Figure 11. $\cos\theta_V$-dependent forward-backward asymmetry defined in (6.8). The upper and lower plots refer to $\ell=\mu$ and $\ell=\tau$, respectively, the left and right column to $F=\pi$ and $F=\gamma$. The solid curves correspond to SM, the dashed ones to NP at the benchmark point $\tilde{\epsilon}_T^\ell$.

$-\cos\theta$, since the first two terms are invariant under this transformation, while the last one changes sign. In F_L this term involves the angular coefficient I_{6c}^π (I_{6s}^γ) proportional to the lepton mass: therefore, the distribution is expected to be nearly symmetric when $\cos\theta \to -\cos\theta$ in the muon case, not for τ. For SM this is shown in figure 12. The analogous plots for F_T are shown in figure 13.

When $F=\pi$, the direction $\cos\theta_V=0$, $\cos\theta=-1$ selects the transverse D^* polarization, while for $\cos\theta_V=\pm1$, $\cos\theta=0$ D^* is longitudinally polarized. For $F=\gamma$, F_L has a maximum at $\cos\theta_V=0$, $\cos\theta=0$, while F_T is largest at $\cos\theta_V=\pm1$, $\cos\theta=-1$. The sensitivity to NP can be visualized integrating the double differential distributions in $\cos\theta$ or in $\cos\theta_V$. At the benchmark point, integrating over $\cos\theta$ we obtain $F_{L,T}(\theta_V)=\int_{-1}^{1} d\cos\theta\, F_{L,T}(\theta,\theta_V)$ in figures 14 and 15. Integrating in $\cos\theta_V$, the distributions $F_{L,T}(\theta)=\int_{-1}^{1} d\cos\theta_V\, F_{L,T}(\theta,\theta_V)$ coincide for $F=\pi$ and $F=\gamma$: they are shown in figure 16 in SM and NP case.

The observables for $\ell=\mu$ are more sensitive to NP: in the case of $F_L(\theta_V)$ the deviation is larger for $\cos\theta_V\simeq\pm1$ for $F=\pi$, and for $\cos\theta_V\simeq0$ for $F=\gamma$. Highest sensitivity to NP is in the function $F_T(\theta)$, which can probe the sign of the angular coefficient I_{2s}^π (I_{2c}^γ) through its concavity. Indeed, the sign of the second derivative of $F_T(\theta)$ with respect to $\cos\theta$ depends on the sign of this coefficient, that is positive in SM but could have a different sign in other scenarios. Indeed, comparing figures 7 and 2 one sees that NP can produce a sign reversal for this coefficient.

JHEP06(2018)082

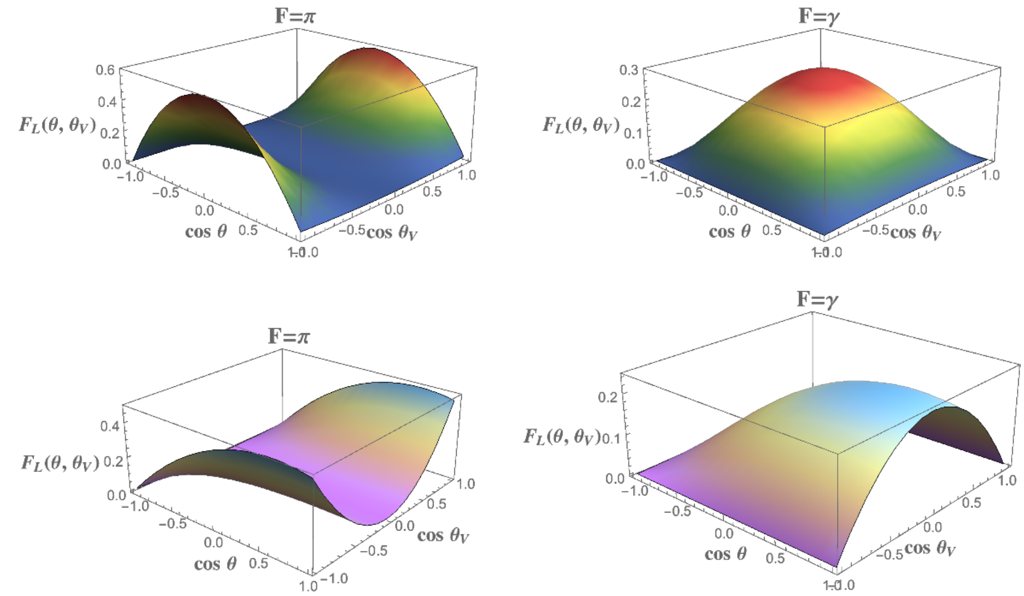

Figure 12. SM distributions $F_L(\theta, \theta_V)$ defined in eq. (6.13). Upper and lower plots refer to $\ell = \mu$ and $\ell = \tau$, respectively, the left and right column to $F = \pi$ and $F = \gamma$.

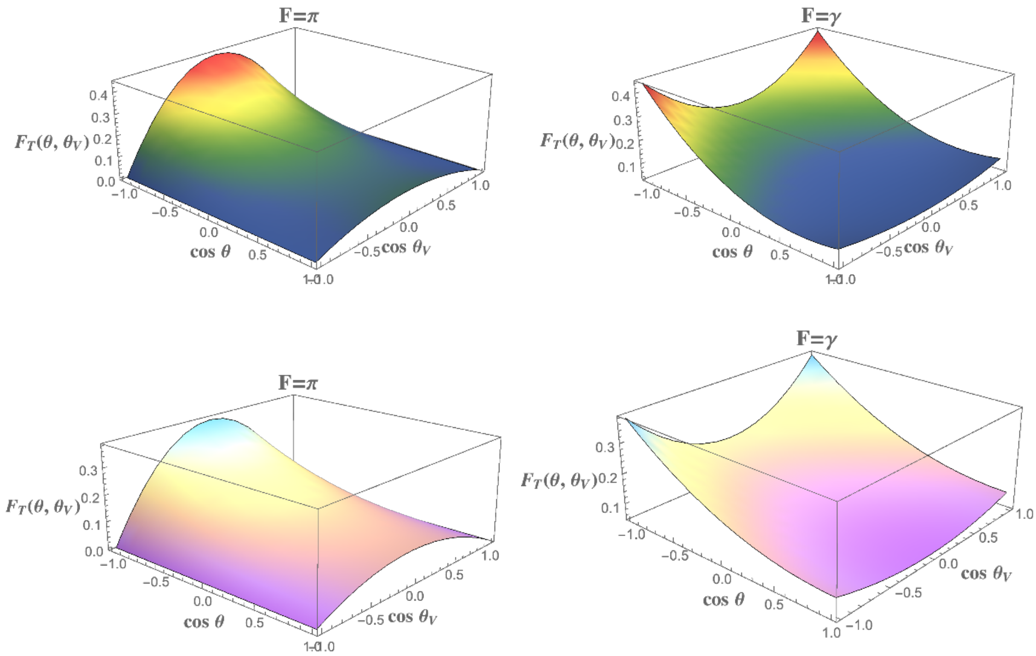

Figure 13. SM distributions $F_T(\theta, \theta_V)$ defined in eq. (6.14). Upper and lower plots refer to $\ell = \mu$ and $\ell = \tau$, respectively, the left and right column to $F = \pi$ and $F = \gamma$.

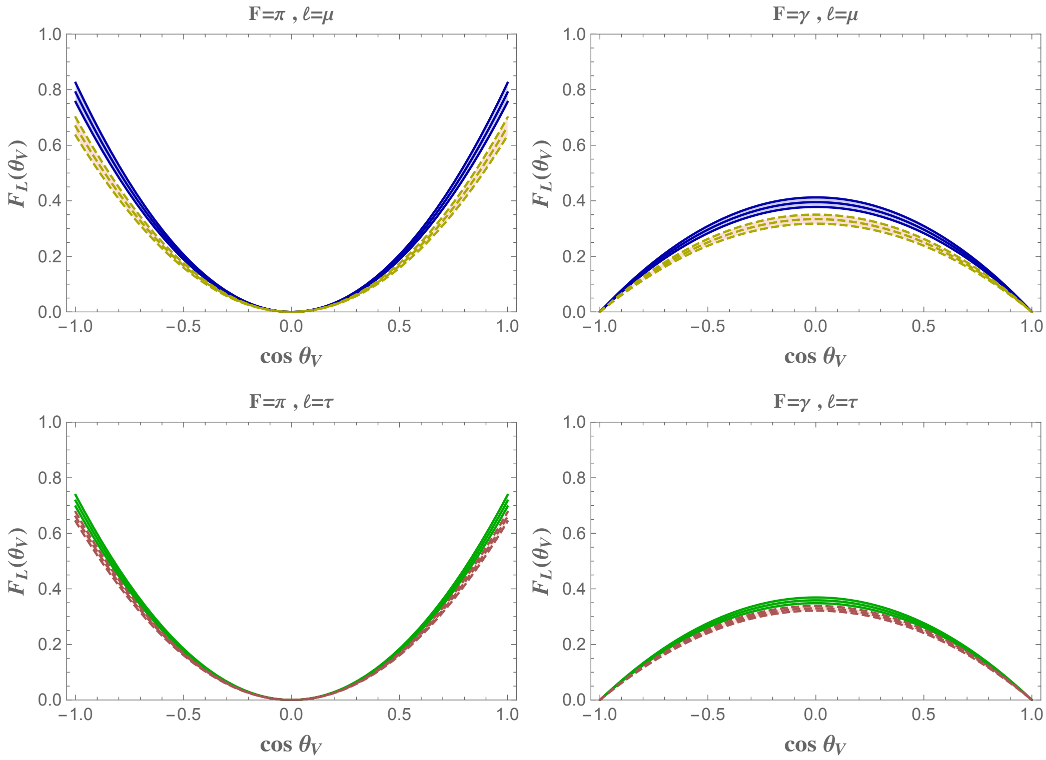

Figure 14. Distribution $F_L(\theta_V)$. The upper and lower plots refer to $\ell = \mu$ and $\ell = \tau$, the left and right column to $F = \pi$ and $F = \gamma$. The continuous lines show the SM result, the dashed lines the NP result at the benchmark point $\tilde{\epsilon}_T^\ell$.

Tests of LFU. The angular coefficient functions in the fully differential distribution provide LFU tests. This is interesting, considering that after integration over the angles only four coefficients contribute to the decay rate, therefore only those are probed by ratios of branching fractions.

Information from the fully differential decay rate can be exploited defining $\tilde{I}_i = \left(1 - \frac{m_\ell^2}{q^2}\right)^2 |\vec{p}_{D^*}|_{BRF}\, I_i$, and the ratios

$$R_i^{\ell_1\,\ell_2} = \frac{\int_{w=1}^{w_{\max}(\ell_1)} (\tilde{I}_i^\pi(w))_{\ell_1} dw}{\int_{w=1}^{w_{\max}(\ell_2)} (\tilde{I}_i^\pi(w))_{\ell_2} dw} \tag{6.15}$$

for $\ell_1\ell_2 = \tau\,\mu, \tau\,e, \mu\,e$. The SM predictions for these ratios, using CLN, are collected in table 2. The errors reflect the form factor uncertainties. Since I_{6c}^π is proportional to the lepton mass squared, the ratios R_{6c}^π are much larger than the others. Analogous ratios in the case of photon can be defined using (3.5). The same quantities predicted in the NP scenario are collected in table 3. In the case of the ratios $R_i^{\mu\,e}$, assuming $\epsilon_T^\mu = \epsilon_T^e$, a deviation with respect to the SM result would signal NP but not LFU violation.

Although the measurement of these ratios is challenging, the high statistics foreseen, e.g., at Belle II is promising [54]. For ratios involving the τ lepton, the use of the τ reconstruction through the three-prong decays, as done at LHCb, can result in improved signal-to-background ratio and in a higher statistical significance [40].

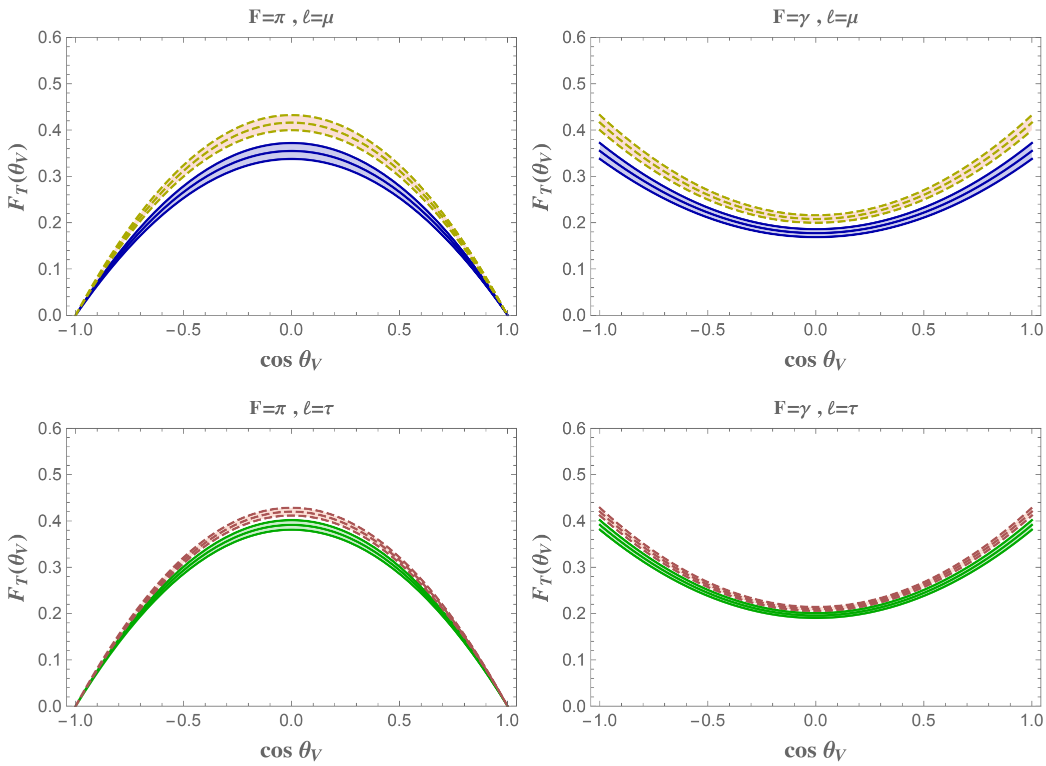

Figure 15. Distribution $F_T(\theta_V)$. The upper and lower plots refer to the case $\ell = \mu$ and $\ell = \tau$, the left and right column to $F = \pi$ and $F = \gamma$. Color codes as in figure 14.

	$\ell_1 = \tau\,,\ \ell_2 = \mu$	$\ell_1 = \tau\,,\ \ell_2 = e$	$\ell_1 = \mu\,,\ \ell_2 = e$
R^π_{1s}	0.263 ± 0.006	0.262 ± 0.005	0.9957 ± 0.0001
R^π_{1c}	0.28 ± 0.02	0.28 ± 0.02	1.008 ± 0.004
R^π_{2s}	0.134 ± 0.003	0.133 ± 0.003	0.9923 ± 0.0002
R^π_{2c}	0.079 ± 0.005	0.077 ± 0.005	0.975 ± 0.002
R^π_3	0.153 ± 0.004	0.152 ± 0.004	0.9932 ± 0.0002
R^π_4	0.112 ± 0.004	0.111 ± 0.004	0.9891 ± 0.0004
R^π_5	0.30 ± 0.02	0.30 ± 0.02	0.999 ± 0.001
R^π_{6s}	0.197 ± 0.004	0.196 ± 0.004	0.9943 ± 0.0001
R^π_{6c}	5.90 ± 0.45	76000 ± 7000	12900 ± 200

Table 2. SM predictions for the ratios in eq. (6.15) using CLN.

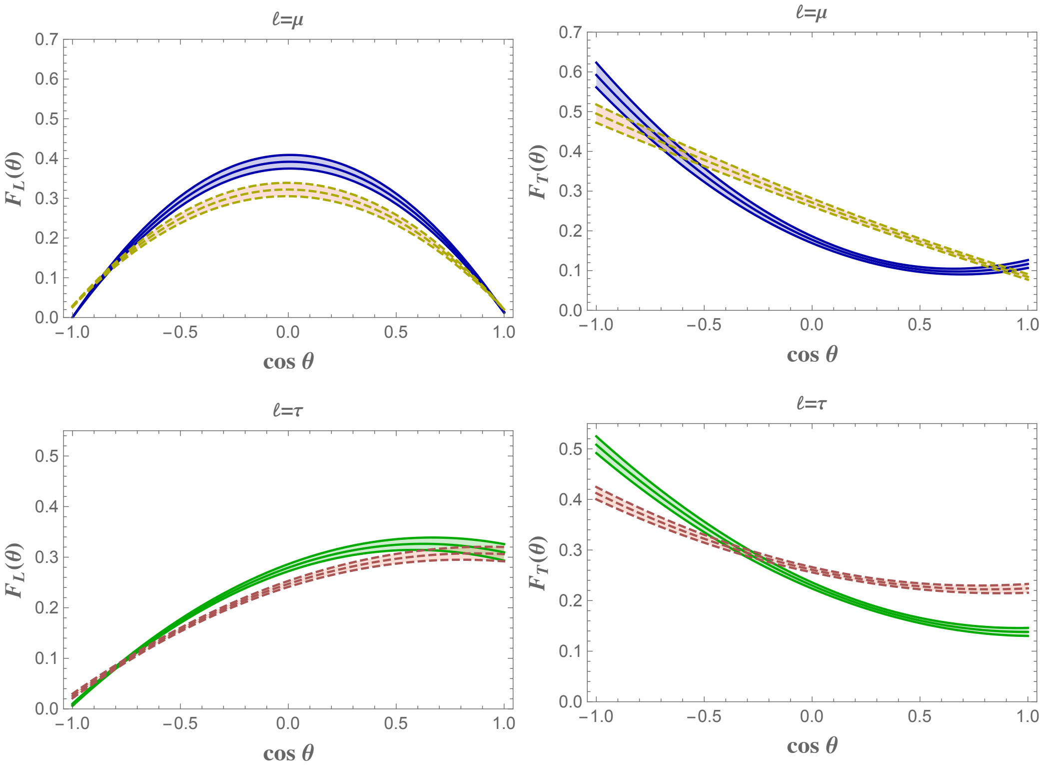

Figure 16. Distributions $F_L(\theta)$ (left) and $F_T(\theta)$ (right). Upper and lower plots refer to $\ell = \mu$ and $\ell = \tau$, respectively. Color codes as in figure 14.

	$\ell_1 = \tau\,,\ \ell_2 = \mu$	$\ell_1 = \tau\,,\ \ell_2 = e$	$\ell_1 = \mu\,,\ \ell_2 = e$
R^{π}_{1s}	0.32 ± 0.01	0.304 ± 0.008	0.957 ± 0.002
R^{π}_{1c}	0.36 ± 0.03	0.34 ± 0.02	0.956 ± 0.003
R^{π}_{2s}	0.37 ± 0.02	0.38 ± 0.02	1.04 ± 0.01
R^{π}_{2c}	0.082 ± 0.006	0.080 ± 0.006	0.973 ± 0.002
R^{π}_{3}	0.183 ± 0.005	0.182 ± 0.005	0.9932 ± 0.0002
R^{π}_{4}	0.131 ± 0.005	0.130 ± 0.005	0.9890 ± 0.0004
R^{π}_{5}	0.35 ± 0.03	0.33 ± 0.03	0.96 ± 0.01
R^{π}_{6s}	0.150 ± 0.006	0.152 ± 0.006	1.012 ± 0.003
R^{π}_{6c}	-11.6 ± 1.5	-944 ± 40	81.2 ± 9.1
R^{π}_{7}	0	0	184 ± 2

Table 3. Ratios (6.15) in the NP scenario with the tensor operator, using CLN and at the benchmark point $\tilde{\epsilon}^{\ell}_T$.

7 Conclusions

To understand the experimental results on semileptonic B decays, the $R(D^{(*)})$ anomaly and the tension in the exclusive vs inclusive $|V_{cb}|$ determinations, it is mandatory to control the uncertainties in the SM predictions and to explore all possible ways in which deviations can be observed. Considering the angular coefficient functions in the fully differential decay distribution in $\bar{B} \to D^* \ell^- \bar{\nu}_\ell$, with D^* decaying either as $D^* \to D\pi$ or as $D^* \to D\gamma$, we have studied several observables able to discern effects of the form factor parametrization and to identify the cases with minimal sensitivity to hadronic uncertainties, useful to pin down deviations. As a testing example, we have considered a NP model with a tensor operator.

Comparing the results obtained using the CLN and the BGL parametrization, we have identified the angular coefficients less sensitive to the parametrization. We have worked out relations allowing to extract the form factors from measured angular coefficients. Moreover, the relations between the angular coefficients for D^* decaying to π and to γ can be used as tests, exploiting the complementary of the two modes.

Considering the SM extension, we have shown that some angular coefficients, absent in the SM, can be found in NP. A number of observables display peculiar features in the NP model, e.g. the q^2-dependent forward-backward asymmetry for τ, and the θ_V-dependent forward-backward asymmetry both for $\ell = \mu$ and for $\ell = \tau$. The D^* transverse polarization fraction $F_T(\theta)$ for $\ell = \mu$ is sensitive to the sign of one of the angular coefficients, different in SM and NP. Finally, ratios to probe LFU and show possible violations have been constructed. Although the measurement of several observables is challenging, in particular in the τ mode, the forthcoming analyses at LHCb and Belle II are surely encouraging and provide exciting perspectives for SM tests and NP searches.

Acknowledgments

We thank C. Bozzi and M. Rotondo for discussions, and M. Jung and D. Straub for comments. This study has been carried out within the INFN project (Iniziativa Specifica) QFT-HEP.

A Four-body phase-space

We remind that the four-body phase-space integration can be carried out using the identities

$$
\begin{aligned}
d\Pi_4 &= \frac{1}{2m_B}[dk_1][dk_2][dp_D][dp_F](2\pi)^4\delta^4(p_B - p_D - p_F - k_1 - k_2) \\
&= \frac{(2\pi)^4}{2m_B}\left\{d^4q d^4p_{D^*}\delta^4(p_B - q - p_{D^*})\right\} \\
&\quad \times \left\{[dk_1][dk_2]\delta^4(q - k_1 - k_2)\right\} \times \left\{[dp_D][dp_F]\delta^4(p_{D^*} - p_D - p_F)\right\} \\
&= \frac{(2\pi)^4}{2m_B} d\Pi_2^{(q,p_{D^*})} \times d\Pi_2^{(k_1,k_2)} \times d\Pi_2^{(p_D,p_F)}\,,
\end{aligned}
\tag{A.1}
$$

using the notation $[dp] = \dfrac{d^3p}{(2\pi)^3 2p^0}$. $d\Pi_2^{(k_1,k_2)}$ and $d\Pi_2^{(p_D,p_F)}$ are the two-body phase-spaces

$$d\Pi_2^{(k_1,k_2)} = \frac{1}{(2\pi)^6}\frac{1}{4\sqrt{q^2}}|\vec{k}_1|_{LRF}\, d\Omega_L \tag{A.2}$$

$$d\Pi_2^{(p_D,p_F)} = \frac{1}{(2\pi)^6}\frac{1}{4\sqrt{p_{D^*}^2}}|\vec{p}_D|_{D^*RF}\, d\Omega_D\,. \tag{A.3}$$

In (A.2), $|\vec{k}_1|_{LRF} = \dfrac{q^2 - m_\ell^2}{2\sqrt{q^2}}$ is the lepton three-momentum in the lepton-pair rest-frame, and $d\Omega_L = d\cos\theta d\phi$. In (A.3), $|\vec{p}_D|_{D^*RF}$ is the D three-momentum in the D^* rest-frame, and $d\Omega_D = (2\pi) d\cos\theta_V$, with θ_V the angle between the D momentum in the D^* rest-frame and the z axis; the integration over the azimuthal angle in this frame is trivial. $d\Pi_2^{(q,p_{D^*})}$ can be evaluated exploiting the narrow width approximation (2.22):

$$d\Pi_2^{(q,p_{D^*})}\delta(p_{D^*}^2 - m_{D^*}^2) = \frac{\pi}{m_B}|\vec{p}_{D^*}|_{BRF}\, dq^2\,, \tag{A.4}$$

where $|\vec{p}_{D^*}|_{BRF}$ is the D^* three-momentum in the B rest-frame.

B Hadronic matrix element parametrizations

In the CLN parametrization [16] the $\bar{B} \to D^*$ matrix elements are written as

$$\begin{aligned}
\langle D^*(v',\epsilon)|\bar{c}\gamma_\mu b|\bar{B}(v)\rangle &= \sqrt{m_B m_{D^*}}\, i\, h_V(w)\epsilon_{\mu\nu\alpha\beta}\epsilon^{*\nu}v'^\alpha v^\beta\,, \\
\langle D^*(v',\epsilon)|\bar{c}\gamma_\mu\gamma_5 b|\bar{B}(v)\rangle &= \sqrt{m_B m_{D^*}}\Big[h_{A_1}(w)(w+1)\epsilon^*_\mu - \left[h_{A_2}(w)v_\mu + h_{A_3}(w)v'_\mu\right](\epsilon^*\cdot v)\Big]\,, \\
\langle D^*(v',\epsilon)|\bar{c}\sigma_{\mu\nu} b|\bar{B}(v)\rangle &= -\sqrt{m_B m_{D^*}}\epsilon_{\mu\nu\alpha\beta}\Big[h_{T_1}(w)\epsilon^{*\alpha}(v+v')^\beta + h_{T_2}(w)\epsilon^{*\alpha}(v-v')^\beta \\
&\qquad + h_{T_3}(w)v^\alpha v'^\beta(\epsilon^*\cdot v)\Big]\,,
\end{aligned} \tag{B.1}$$

with v and v' the B and D^* four-velocities and $w = v\cdot v'$. The factor $\sqrt{m_B m_{D^*}}$ accounts for the mass-dependent normalization of the states (in [16] the mass-independent normalization is adopted). This parametrization is related to the one in (2.24)–(2.25) through

$$\begin{aligned}
V(q^2) &= \frac{m_B + m_{D^*}}{2\sqrt{m_B m_{D^*}}} h_V(w) \\
A_1(q^2) &= \sqrt{m_B m_{D^*}}\frac{w+1}{m_B + m_{D^*}} h_{A_1}(w) \\
A_2(q^2) &= \frac{m_B + m_{D^*}}{2\sqrt{m_B m_{D^*}}}\left[h_{A_3}(w) + \frac{m_{D^*}}{m_B}h_{A_2}(w)\right] \\
A_0(q^2) &= \frac{1}{2\sqrt{m_B m_{D^*}}}\left[m_B(w+1)h_{A_1}(w) - (m_B - m_{D^*}w)h_{A_2}(w) - (m_B w - m_{D^*})h_{A_3}(w)\right],
\end{aligned} \tag{B.2}$$

and

$$
\begin{aligned}
T_0(q^2) &= -\frac{(m_B + m_{D^*})^2}{m_B m_{D^*}} \sqrt{\frac{m_{D^*}}{m_B}} h_{T_3}(w) \\
T_1(q^2) &= \sqrt{\frac{m_{D^*}}{m_B}} \left(h_{T_1}(w) + h_{T_2}(w)\right) \\
T_2(q^2) &= \sqrt{\frac{m_B}{m_{D^*}}} \left(h_{T_1}(w) - h_{T_2}(w)\right) ,
\end{aligned}
\tag{B.3}
$$

with $q^2 = m_B^2 + m_{D^*}^2 - 2m_B m_{D^*} w$. The form factors T_3, T_4, T_5 in (2.25) are related to T_0, T_1, T_2 by the identity: $\sigma_{\mu\nu}\gamma_5 = \frac{i}{2}\epsilon_{\mu\nu\alpha\beta}\sigma^{\alpha\beta}$. The relations of the form factors in (B.1) to the Isgur-Wise function, $h_V(w) = h_{A_1}(w) = h_{A_3}(w) = h_{T_1}(w) = \xi(w)$ and $h_{A_2} = h_{T_2} = h_{T_3} = 0$ hold in the HQ limit. Such relations can be improved including radiative α_s and power $\frac{1}{m_b}$, $\frac{1}{m_c}$ corrections. In the case of the functions in (B.2) they have been worked out in [16, 53]:

$$
\begin{aligned}
h_V(w) &= \left[C_1 + \epsilon_c(L_2 - L_5) + \epsilon_b(L_1 - L_4)\right] \xi(w) \\
h_{A_1}(w) &= \left[C_1^5 + \epsilon_c\left(L_2 - \frac{w-1}{w+1}L_5\right) + \epsilon_b\left(L_1 - \frac{w-1}{w+1}L_4\right)\right] \xi(w) \\
h_{A_2}(w) &= \left[C_2^5 + \epsilon_c(L_3 + L_6)\right] \xi(w) \\
h_{A_3}(w) &= \left[C_1^5 + C_3^5 + \epsilon_c(L_2 - L_3 - L_5 + L_6) + \epsilon_b(L_1 - L_4)\right] \xi(w) \,.
\end{aligned}
\tag{B.4}
$$

The coefficients C_i incorporate the radiative corrections. L_i account for $\mathcal{O}(1/m_Q)$ corrections in the HQ expansion, and their numerical values have been obtained using QCD sum rule determinations of the subleading form factors [53]. Their expressions can be found in the original papers [16, 53], and are collected in the appendix of [24]. The analogous relations for the form factors in (B.3) have been worked out in [12]:

$$
\begin{aligned}
h_{T_1}(w) &= \left[\tilde{C}_1 + \epsilon_c L_2 + \epsilon_b L_1\right] \xi(w) \\
h_{T_2}(w) &= \left[\tilde{C}_2 + \epsilon_c L_5 - \epsilon_b L_4\right] \xi(w) \\
h_{T_3}(w) &= \left[\tilde{C}_3 + \epsilon_c(L_6 - L_3)\right] \xi(w)
\end{aligned}
\tag{B.5}
$$

where $\tilde{C}_i$ incorporate the radiative corrections. Among the C_i and $\tilde{C}_i$, the set C_2^5, $\tilde{C}_2$ and $\tilde{C}_3$ starts at $\mathcal{O}(\alpha_s)$. We refer to [12] for the expressions of the parameters in (B.5).

The BGL parametrization uses the form factors g, f, a_+ and a_-:

$$
\begin{aligned}
\langle D^*(p',\epsilon)|\bar{c}\gamma_\mu b|\bar{B}(p)\rangle &= i\,\epsilon_{\mu\nu\alpha\beta}\epsilon^{*\nu}p'^{\alpha}p^{\beta} g \,, \\
\langle D^*(v',\epsilon)|\bar{c}\gamma_\mu\gamma_5 b|\bar{B}(v)\rangle &= \epsilon^*_\mu f + (\epsilon^*\cdot p)\left[(p+p')_\mu a_+ + (p-p'_\mu)a_-\right] ,
\end{aligned}
\tag{B.6}
$$

so that

$$
\begin{aligned}
g(w) &= \frac{h_V(w)}{\sqrt{m_B m_{D^*}}} \\
f(w) &= \sqrt{m_B m_{D^*}}(1+w)h_{A_1}(w) \\
a_+(w) &= -\frac{m_{D^*}}{2\sqrt{m_B m_{D^*}}}\left(\frac{h_{A_3}(w)}{m_{D^*}} + \frac{h_{A_2}(w)}{m_B}\right) \\
a_-(w) &= \frac{m_{D^*}}{2\sqrt{m_B m_{D^*}}}\left(\frac{h_{A_3}(w)}{m_{D^*}} - \frac{h_{A_2}(w)}{m_B}\right).
\end{aligned}
\tag{B.7}
$$

The expressions of the helicity amplitudes are:

$$
\begin{aligned}
H_0 &= \frac{\mathcal{F}_1(w)}{\sqrt{q^2}} \\
H_\pm &= f(w) \mp m_B m_{D^*}\sqrt{w^2-1}\, g(w)\,,
\end{aligned}
\tag{B.8}
$$

with

$$
\mathcal{F}_1(w) = \sqrt{m_B m_{D^*}}(1+w)\left[(m_B w - m_{D^*})h_{A_1}(w) - m_{D^*}(w-1)h_{A_2}(w) - m_B(w-1)h_{A_3}(w)\right].
$$

In the BGL approach, the observation is used that the W production amplitude of $\bar{B}\bar{D}^*$ is related to the $\bar{B} \to D^*$ form factors by analytic continuation from the semileptonic region $m_\ell^2 \le t \le t_-$ to the region $t_+ \le t$, with $t_\pm = (m_B \pm m_{D^*})^2$ [18–20]. In the production region, constraints can be imposed using perturbative QCD, including quark and gluon condensate corrections. Then, analyticity is exploited. The form factors are written as functions of the conformal variable z in the form: $f(z) = \frac{1}{P_f(z)\phi_f(z)} \sum_{n=0}^{N} a_n z^n$. The Blatsche factors $P_f(z)$ account for the $t < (m_B + m_{D^*})^2$ poles associated with on-shell production of $\bar{c}b$ bound states, while $\phi_f(z)$ are outer functions from phase-space integration. The coefficients a_n satisfy unitarity bounds of the type $\sum_{n=0}^{N} |a_n|^2 \le 1$. For $B \to D^*$, three coefficients a_n, with $n = 0, 1, 2$, have been fitted for each form factor g, f and $\mathcal{F}_1$ [21], and unitarity bounds have been imposed [10]. The masses of the $\bar{c}b$ lowest-lying bound states with suitable J^P quantum numbers are taken from constituent quark models. The resulting values of the parameters are reported in [21]: they are used in our analysis.

References

[1] HFLAV collaboration, Y. Amhis et al., *Averages of b-hadron, c-hadron, and τ-lepton properties as of summer 2016*, *Eur. Phys. J.* **C 77** (2017) 895 [arXiv:1612.07233] [INSPIRE].

[2] BaBar collaboration, J.P. Lees et al., *Evidence for an excess of $\bar{B} \to D^{(*)}\tau^-\bar{\nu}_\tau$ decays*, *Phys. Rev. Lett.* **109** (2012) 101802 [arXiv:1205.5442] [INSPIRE].

[3] BaBar collaboration, J.P. Lees et al., *Measurement of an Excess of $\bar{B} \to D^{(*)}\tau^-\bar{\nu}_\tau$ Decays and Implications for Charged Higgs Bosons*, Phys. Rev. **D 88** (2013) 072012 [arXiv:1303.0571] [INSPIRE].

[4] Belle collaboration, M. Huschle et al., *Measurement of the branching ratio of $\bar{B} \to D^{(*)}\tau^-\bar{\nu}_\tau$ relative to $\bar{B} \to D^{(*)}\ell^-\bar{\nu}_\ell$ decays with hadronic tagging at Belle*, Phys. Rev. **D 92** (2015) 072014 [arXiv:1507.03233] [INSPIRE].

[5] Belle collaboration, Y. Sato et al., *Measurement of the branching ratio of $\bar{B}^0 \to D^{*+}\tau^-\bar{\nu}_\tau$ relative to $\bar{B}^0 \to D^{*+}\ell^-\bar{\nu}_\ell$ decays with a semileptonic tagging method*, Phys. Rev. **D 94** (2016) 072007 [arXiv:1607.07923] [INSPIRE].

[6] Belle collaboration, S. Hirose et al., *Measurement of the τ lepton polarization and $R(D^*)$ in the decay $\bar{B} \to D^*\tau^-\bar{\nu}_\tau$*, Phys. Rev. Lett. **118** (2017) 211801 [arXiv:1612.00529] [INSPIRE].

[7] LHCb collaboration, *Measurement of the ratio of branching fractions $\mathcal{B}(\bar{B}^0 \to D^{*+}\tau^-\bar{\nu}_\tau)/\mathcal{B}(\bar{B}^0 \to D^{*+}\mu^-\bar{\nu}_\mu)$*, Phys. Rev. Lett. **115** (2015) 111803 [arXiv:1506.08614] [INSPIRE].

[8] S. Fajfer, J.F. Kamenik and I. Nisandzic, *On the $B \to D^*\tau\bar{\nu}_\tau$ Sensitivity to New Physics*, Phys. Rev. **D 85** (2012) 094025 [arXiv:1203.2654] [INSPIRE].

[9] S. Aoki et al., *Review of lattice results concerning low-energy particle physics*, Eur. Phys. J. **C 77** (2017) 112 [arXiv:1607.00299] [INSPIRE].

[10] D. Bigi, P. Gambino and S. Schacht, *$R(D^*)$, $|V_{cb}|$, and the Heavy Quark Symmetry relations between form factors*, JHEP **11** (2017) 061 [arXiv:1707.09509] [INSPIRE].

[11] S. Jaiswal, S. Nandi and S.K. Patra, *Extraction of $|V_{cb}|$ from $B \to D^{(*)}\ell\nu_\ell$ and the Standard Model predictions of $R(D^{(*)})$*, JHEP **12** (2017) 060 [arXiv:1707.09977] [INSPIRE].

[12] F.U. Bernlochner, Z. Ligeti, M. Papucci and D.J. Robinson, *Combined analysis of semileptonic B decays to D and D^*: $R(D^{(*)})$, $|V_{cb}|$, and new physics*, Phys. Rev. **D 95** (2017) 115008 [arXiv:1703.05330] [INSPIRE].

[13] Belle collaboration, S. Hirose et al., *Measurement of the τ lepton polarization and $R(D^*)$ in the decay $\bar{B} \to D^*\tau^-\bar{\nu}_\tau$ with one-prong hadronic τ decays at Belle*, Phys. Rev. **D 97** (2018) 012004 [arXiv:1709.00129] [INSPIRE].

[14] LHCb collaboration, *Measurement of the ratio of branching fractions $\mathcal{B}(B_c^+ \to J/\psi\tau^+\nu_\tau)/\mathcal{B}(B_c^+ \to J/\psi\mu^+\nu_\mu)$*, Phys. Rev. Lett. **120** (2018) 121801 [arXiv:1711.05623] [INSPIRE].

[15] C.-T. Tran, M.A. Ivanov, J.G. Körner and P. Santorelli, *Implications of new physics in the decays $B_c \to (J/\psi, \eta_c)\tau\nu$*, Phys. Rev. **D 97** (2018) 054014 [arXiv:1801.06927] [INSPIRE].

[16] I. Caprini, L. Lellouch and M. Neubert, *Dispersive bounds on the shape of $\bar{B} \to D^{(*)}$ lepton anti-neutrino form-factors*, Nucl. Phys. **B 530** (1998) 153 [hep-ph/9712417] [INSPIRE].

[17] Belle collaboration, A. Abdesselam et al., *Precise determination of the CKM matrix element $|V_{cb}|$ with $\bar{B}^0 \to D^{*\,+}\,\ell^-\,\bar{\nu}_\ell$ decays with hadronic tagging at Belle*, arXiv:1702.01521 [INSPIRE].

[18] C.G. Boyd, B. Grinstein and R.F. Lebed, *Constraints on form-factors for exclusive semileptonic heavy to light meson decays*, Phys. Rev. Lett. **74** (1995) 4603 [hep-ph/9412324] [INSPIRE].

JHEP06(2018)082

[19] C.G. Boyd, B. Grinstein and R.F. Lebed, *Model independent extraction of $|V_{cb}|$ using dispersion relations*, Phys. Lett. **B 353** (1995) 306 [hep-ph/9504235] [INSPIRE].

[20] C.G. Boyd, B. Grinstein and R.F. Lebed, *Model independent determinations of $\bar{B} \to D$ (lepton), D^* (lepton) anti-neutrino form-factors*, Nucl. Phys. **B 461** (1996) 493 [hep-ph/9508211] [INSPIRE].

[21] D. Bigi, P. Gambino and S. Schacht, *A fresh look at the determination of $|V_{cb}|$ from $B \to D^* \ell \nu$*, Phys. Lett. **B 769** (2017) 441 [arXiv:1703.06124] [INSPIRE].

[22] B. Grinstein and A. Kobach, *Model-Independent Extraction of $|V_{cb}|$ from $\bar{B} \to D^* \ell \bar{\nu}$*, Phys. Lett. **B 771** (2017) 359 [arXiv:1703.08170] [INSPIRE].

[23] P. Colangelo and F. De Fazio, *Tension in the inclusive versus exclusive determinations of $|V_{cb}|$: a possible role of new physics*, Phys. Rev. **D 95** (2017) 011701 [arXiv:1611.07387] [INSPIRE].

[24] P. Biancofiore, P. Colangelo and F. De Fazio, *Anomalous enhancement observed in $B \to D^{(*)} \tau \bar{\nu}_\tau$ decays*, Phys. Rev. **D 87** (2013) 074010 [arXiv:1302.1042] [INSPIRE].

[25] M. Duraisamy and A. Datta, *The Full $B \to D^* \tau^- \bar{\nu}_\tau$ Angular Distribution and CP violating Triple Products*, JHEP **09** (2013) 059 [arXiv:1302.7031] [INSPIRE].

[26] S. Bhattacharya, S. Nandi and S.K. Patra, *Optimal-observable analysis of possible new physics in $B \to D^{(*)} \tau \nu_\tau$*, Phys. Rev. **D 93** (2016) 034011 [arXiv:1509.07259] [INSPIRE].

[27] D. Bardhan, P. Byakti and D. Ghosh, *A closer look at the R_D and R_{D^*} anomalies*, JHEP **01** (2017) 125 [arXiv:1610.03038] [INSPIRE].

[28] R. Alonso, A. Kobach and J. Martin Camalich, *New physics in the kinematic distributions of $\bar{B} \to D^{(*)} \tau^- (\to \ell^- \bar{\nu}_\ell \nu_\tau) \bar{\nu}_\tau$*, Phys. Rev. **D 94** (2016) 094021 [arXiv:1602.07671] [INSPIRE].

[29] D. Bečirević, S. Fajfer, I. Nisandzic and A. Tayduganov, *Angular distributions of $\bar{B} \to D^{(*)} \ell \bar{\nu}_\ell$ decays and search of New Physics*, arXiv:1602.03030 [INSPIRE].

[30] Z. Ligeti, M. Papucci and D.J. Robinson, *New Physics in the Visible Final States of $B \to D^{(*)} \tau \nu$*, JHEP **01** (2017) 083 [arXiv:1610.02045] [INSPIRE].

[31] A.K. Alok, D. Kumar, S. Kumbhakar and S.U. Sankar, *D^* polarization as a probe to discriminate new physics in $\bar{B} \to D^* \tau \bar{\nu}$*, Phys. Rev. **D 95** (2017) 115038 [arXiv:1606.03164] [INSPIRE].

[32] M.A. Ivanov, J.G. Körner and C.-T. Tran, *Probing new physics in $\bar{B}^0 \to D^{(*)} \tau^- \bar{\nu}_\tau$ using the longitudinal, transverse, and normal polarization components of the tau lepton*, Phys. Rev. **D 95** (2017) 036021 [arXiv:1701.02937] [INSPIRE].

[33] R. Alonso, J. Martin Camalich and S. Westhoff, *Tau properties in $B \to D \tau \nu$ from visible final-state kinematics*, Phys. Rev. **D 95** (2017) 093006 [arXiv:1702.02773] [INSPIRE].

[34] M. Jung and D.M. Straub, *Constraining new physics in $b \to c \ell \nu$ transitions*, arXiv:1801.01112 [INSPIRE].

[35] M. Bauer and M. Neubert, *Minimal Leptoquark Explanation for the $R_{D^{(*)}}$, R_K, and $(g-2)_g$ Anomalies*, Phys. Rev. Lett. **116** (2016) 141802 [arXiv:1511.01900] [INSPIRE].

[36] D. Bečirević, S. Fajfer, N. Košnik and O. Sumensari, *Leptoquark model to explain the B-physics anomalies, R_K and R_D*, Phys. Rev. **D 94** (2016) 115021 [arXiv:1608.08501] [INSPIRE].

JHEP06(2018)082

[37] A. Crivellin, D. Müller and T. Ota, *Simultaneous explanation of $R(D^{(*)})$ and $b \to s\mu^+\mu^-$: the last scalar leptoquarks standing*, *JHEP* **09** (2017) 040 [arXiv:1703.09226] [INSPIRE].

[38] D. Buttazzo, A. Greljo, G. Isidori and D. Marzocca, *B-physics anomalies: a guide to combined explanations*, *JHEP* **11** (2017) 044 [arXiv:1706.07808] [INSPIRE].

[39] F. Feruglio, P. Paradisi and A. Pattori, *On the Importance of Electroweak Corrections for B Anomalies*, *JHEP* **09** (2017) 061 [arXiv:1705.00929] [INSPIRE].

[40] LHCb collaboration, *Test of Lepton Flavor Universality by the measurement of the $B^0 \to D^{*-}\tau^+\nu_\tau$ branching fraction using three-prong τ decays*, *Phys. Rev.* **D 97** (2018) 072013 [arXiv:1711.02505] [INSPIRE].

[41] J.G. Körner and G.A. Schuler, *Exclusive Semileptonic Heavy Meson Decays Including Lepton Mass Effects*, *Z. Phys.* **C 46** (1990) 93 [INSPIRE].

[42] F.J. Gilman and R.L. Singleton, *Analysis of Semileptonic Decays of Mesons Containing Heavy Quarks*, *Phys. Rev.* **D 41** (1990) 142 [INSPIRE].

[43] M. González-Alonso, J. Martin Camalich and K. Mimouni, *Renormalization-group evolution of new physics contributions to (semi)leptonic meson decays*, *Phys. Lett.* **B 772** (2017) 777 [arXiv:1706.00410] [INSPIRE].

[44] C.F. Uhlemann and N. Kauer, *Narrow-width approximation accuracy*, *Nucl. Phys.* **B 814** (2009) 195 [arXiv:0807.4112] [INSPIRE].

[45] C.G. Boyd, B. Grinstein and R.F. Lebed, *Precision corrections to dispersive bounds on form-factors*, *Phys. Rev.* **D 56** (1997) 6895 [hep-ph/9705252] [INSPIRE].

[46] A. Vaquero Avilés-Casco et al., *$\overline{B} \to D^*\ell\overline{\nu}$ at Non-Zero Recoil*, *EPJ Web Conf.* **175** (2018) 13003 [arXiv:1710.09817] [INSPIRE].

[47] F.U. Bernlochner, Z. Ligeti, M. Papucci and D.J. Robinson, *Tensions and correlations in $|V_{cb}|$ determinations*, *Phys. Rev.* **D 96** (2017) 091503 [arXiv:1708.07134] [INSPIRE].

[48] Fermilab Lattice and MILC collaborations, J.A. Bailey et al., *Update of $|V_{cb}|$ from the $\bar{B} \to D^*\ell\bar{\nu}$ form factor at zero recoil with three-flavor lattice QCD*, *Phys. Rev.* **D 89** (2014) 114504 [arXiv:1403.0635] [INSPIRE].

[49] A. Sirlin, *Large m_W, m_Z Behavior of the $O(\alpha)$ Corrections to Semileptonic Processes Mediated by W*, *Nucl. Phys.* **B 196** (1982) 83 [INSPIRE].

[50] D. Atwood and W.J. Marciano, *Radiative Corrections and Semileptonic B Decays*, *Phys. Rev.* **D 41** (1990) 1736 [INSPIRE].

[51] MILC collaboration, J.A. Bailey et al., *$B \to D$ form factors at nonzero recoil and $|V_{cb}|$ from 2+1-flavor lattice QCD*, *Phys. Rev.* **D 92** (2015) 034506 [arXiv:1503.07237] [INSPIRE].

[52] Belle collaboration, W. Dungel et al., *Measurement of the form factors of the decay $B^0 \to D^{*-}\ell^+\nu$ and determination of the CKM matrix element $|V_{cb}|$*, *Phys. Rev.* **D 82** (2010) 112007 [arXiv:1010.5620] [INSPIRE].

[53] M. Neubert, *Heavy quark symmetry*, *Phys. Rept.* **245** (1994) 259 [hep-ph/9306320] [INSPIRE].

[54] BELLE-II collaboration, E. Guido, *Belle II physics prospects*, PoS(FPCP2017)036.